TRANSMISSION LINE SIMULATION

FOR

TRANSIENT NETWORK ANALYSER AT VIRGINIA TECH

by

Robert L. Dellinger

Thesis submitted to the Faculty of the

Virginia Polytechnic Institute and State University

in partial fulfillment of the requirements for the degree of

MASTER OF SCIENCE

in

Electrical Engineering

APPROVED:

A. G. Phadke, Chairman

L. L. Grigsby

F. C. Brockhurst

December 1983

Blacksburg, Virginia

TRANSMISSION LINE SIMULATION

FOR

TRANSIENT NETWORK ANALYSER AT VIRGINIA TECH

by

Robrert L. Dellinger

(Abstract)

A general purpose cascaded pi section representation of a transmission line for a Transient Network Analyzer was designed. The pi sections modeled single and double circuit lines at 34.5, 69, 138, 345 and 765 KV levels. Representations of mutual impedances produced by nontransposition and mutual impedances and electrostatic coupling in double circuit lines are included in the model.

Line data was collected for the above mentioned transmission line configurations. Impedance and capacitance matrices were calculated for each line. The matices were scaled to model voltage levels. Equations were derived relating these matrices to model cpmponent values. Inductors were designed for the model. Finally, the pi sections were built and tested.

Test results indicate steady state responses were

generally correct to five percent. Maximum steady state error measured was 8.6 percent. Results from the transient response tests were indicative of lines represented by very few pi sections.

Acknowledgments

I would like to take the opportunity to thank those who have helped to make this thesis possible. First, I would like to thank Dr. A. G. Phadke for his guidance and help in all phases of this project. I would also like to thank Dr. L. L. Grigsby for his guidance and encouragement in the early part of this work.

Thanks also to Dave Jennings, my supervisor at work, for allowing the many interruptions to my work at Va. Tech Electric Service. I would also like to express my appreciation to the Energy Research Group and to the Pratt Fellowship for their funding during my first year of graduate school. Finally thanks also to my wife, Carole for her love, encouragement and help during this time.

TABLE OF CONTENTS

List of Figures

List of Figures (continued)

List of Tables

List of Tables (continued)

I. INTRODUCTION

As power systems have grown the need for accurate modeling of the systems has also grown. System modeling is necessary for studying all types of system problems such as load flow, short circuit analysis, switching and lightning surges,and transient stability studies. The four approaches which have been developed for system modeling are physical analog modeling, analog computer modeling, digital computer modeling, and hybrid computer modeling.

Physical analog models were the earliest models employed. DC network analysers were first employed to give approximate values for short circuits [7]. Need for greater accuracy resulted in AC network analysers and continued improvement in the elements being modelled. Present day Transient Network Analysers (TNA) provide the accuracy needed for transient studies of power systems. Transient Network Analysers now include representation of electromagnetic and electrostactic coupling of untransposed and double circuit lines, magnetic saturation of transformers, nonlinear surge arrestors, and models of circuit breakers and generators [9].

The advent of digital computers gave power system engineers the capability of representing the power system elements mathematically and solving the large number of equations involved in power system modeling[1,2].

Hybrid simulators often use analog computer elements to

represent the many nonlinear elements and to integrate the differential equations of the power system. The digital computer solves equations of the linear elements of the system and the transport delay functions which represent ideal transmission lines [10].

The need for accurate simulation of all types of power system problems is necessary in the design phase to produce the most economic and sound design. In operational studies accurate simulation is needed to solve specific operating problems. Switching and lightning surge studies can predict what kind of overvoltages will be present on system elements. This information is then used in designing insulation coordination for the system. Short circuit analysis demonstrates the magnitudes of fault currents possible on a system. Ratings of power apparatus and system relay design and coordination can then be planned accordingly. Locations for new plants, lines, and interconections can be evaluated and their effect on system stability can be determined before any constructon is begun.

Today, the steady state problems of load flow and short circuit analysis are routinely performed using the digital computer [7]. Transient stability studies are done with the digital computer or with hybrid models, while the Transient Network Analyser (TNA) is most often used for overvoltage studies. The nonlinear effects and frequency dependent parameters of such elements as surge arrestors make digital

simulation much more challenging today.

There are several characteristics that make a physical model attractive. Other physical equipment such as metering systems, control systems, and protective relays can be connected directly to the model. Also, it simulates phenomena in real time, thus critical timing relationships are maintained in the model. The model can maintain a steady state indefinitely. There is no counterpart to the "integration error" which prevails in computer models. These features also make a physical model useful as a training and educational tool.

The power system simulator at Virginia Tech will be of the physical analog model TNA type. It will include representations of generators, transformers, circuit breakers, and transmission lines. Somewhat similar facilities exist at several industrial labs around the world. This paper will concentrate on the design and construction of the line section elements.

II. LINES TO BE MODELED

The line section element of the power system simulator is a pi type representation of a transmision line. The line to be modeled would be made up of several sections joined together to make the actual length of the line.

The major high voltage levels in the country are 34.5, 45, 69, 115, and 230 kilovolts. The major extra high voltage levels are 345, 500, 765, and 1100 kilovolts. As voltage level increases, the conductor size and spacing increase, with conductor bundling being used at the EHV levels. From these the following type of lines were selected to be modeled:

1. 765 kv single circuit line section
2. 345 kv single and double circuit line
3. 138 kv single and double circuit line
4. 69 kv single and double circuit line
5. 34.5 kv single and double circuit line

Line data for each of the circuit types listed above was obtained from the American Electric Power Service Corporation (AEP) for actual AEP lines. It will be used in this model as a representation of those classes of transmission lines. This information included tower configurations, conductor sizes and types,and conductor sag. This line data was used as input data for the Electromagnetic Transient Analysis Program (EMTP). This program calculated the line impedance and charging susceptance matrices and the positive and zero sequence propagation velocities for each line.

The EMTP program uses the following equations and assumptions [11] in calculating the impedance and admittance matrices. The program uses Carson's formula [5] for calculating the impedance matrix. It is assumed that conductor spacing is large enough so that the proximity effect is negligible and that the conductors are long enough so that end effects are negligible. Also, the earth is assumed to have a uniform conductivity. The diagonal elements of [Z] given by equation (1) below are the self impedances. The off-diagonal elements given by equation (2) are the mutual impedances. The resulting impedance elements are in ohms/km.

$$Z(ii) = \left(R(ii) + \Delta R(ii) + j \left(2\omega \cdot 10^{-4} \ln \frac{2h(i)}{GMR(i)} + \Delta X(ii)\right)\right) \quad (1)$$

$$Z(ik) = Z(ki) = R(ik) + j \left(2\omega \cdot 10^{-4} \ln \frac{S(ik)}{s(ik)} + \Delta X(ik)\right) \quad (2)$$

where

R(ii) = resistance of conductor i in ohm/km
h(i) = height of conductor i above ground
S(ik) = distance between conductor i and image of conductor k
s(ik) = distance between conductor i and k
GMR(i) = geometric mean radius of conductor i
$\omega = 2 \cdot \pi \cdot f$ with f=frequency in hertz

Carson developed an infinite integral for the earth return correction terms, ΔR and ΔX. These terms are functions of the angle ϕ: $\phi=0$ for self impedance, $\phi=\phi(ik)$ (Fig. 1) for mutual impedance, and the parameter 'a' which

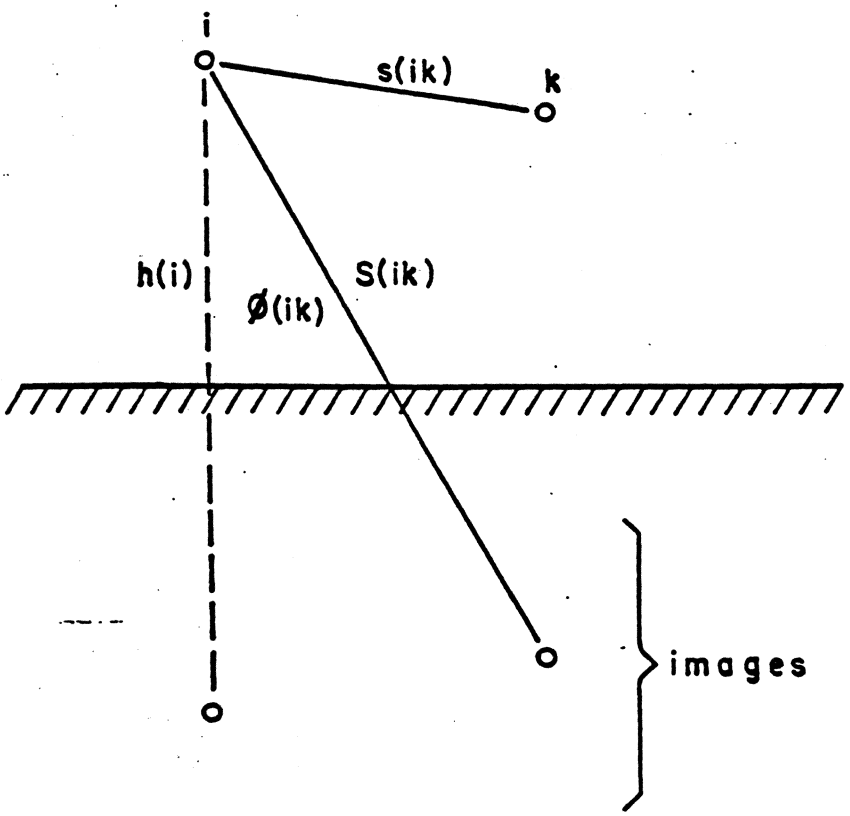

Fig. 1 Conductor Images

is defined as follows:

$$a = k \cdot S \cdot (f/\rho) \qquad (3)$$

$$k = 4 \cdot \pi \cdot \sqrt{5} \cdot 10^{-4} \qquad (4)$$

where

S = 2h(i) in m. (for self impedance)
S = S(ik) in m. (for mutual impedance)
ρ = earth resistivity in ohm-m.

For $a \leq 5$, the infinite integral is developed into an infinite series. The EMTP program computes as many terms of the infiite series as is needed to converge to a given tolerance. For $a > 5$, another finite series approximation is used.

The shunt capacitance matrix [C] is the inverse of the matrix [P] of the potential coefficients, equation (5).

$$[C] = [P^{-1}] \qquad (5)$$

The elements of [P] are calculated from the geometry of the line. The diagonal elements are given by equation (6). The off-diagonal elements are given by equation (7). It is assumed that the conductor spacings are large compared to the conductor radii. The resulting elements of [P] are in daraf-km.

$$P(ii) = 18 \cdot 10^{6} \ln\frac{2\,h(i)}{r(i)} \qquad (6)$$

$$P(ik) = 18 \cdot 10^{6} \ln\frac{S(ik)}{s(ik)} \qquad (7)$$

where

r(i) = radius of conductor i
S(ik), s(ik), and h(i) are defined above

Output quantities from the program are in ohms/mile for impedance matrices and mhos/mile for the susceptance matrices. An earth resistivity of 100 ohm-meter was used for all lines studied. Constants for several lines from each voltage level were calculated. A typical line was then selected from these to represent each circuit type.

The line impedance and charging susceptance matrices produced included the unequal mutual impedances produced by nontransposition of the lines. It also included the mutual impedances between double circuit lines and electrostatic coupling between all conductors.

The pi type line section was designed to account for effects of nontransposition as well as the mutual coupling between parallel circuits.

III. TRANSMISSION LINE SIMULATION THEORY

An important consideration is the error involved in using cascaded pi sections to represent a transmission line. The following derivation [8] for a single phase line will give some idea of the problem.

For the pi section of Figure 2, the admittances and impedances are related by equations (8) and (9). The driving point and transfer admittances and impedances are given by (10) through (13). Driving point and transfer admittances are calculated as a ratio of a current to a voltage with one end of the section shorted.

$$Z1 = \frac{1}{Y1} \tag{8}$$

$$Z2 = \frac{1}{Y2} \tag{9}$$

$$y11 = \frac{I1}{E1} = y22 = \frac{I2}{E2} = \frac{Y2}{2} + Y1 \tag{10}$$

$$y12 = \frac{I2}{E2} = y21 = \frac{I2}{E1} = -Y1 \tag{11}$$

$$z11 = z22 = \frac{y11}{y11^2 - y12^2} \tag{12}$$

$$z12 = z21 = \frac{y12}{y11^2 - y12^2} \tag{13}$$

Writing current and voltage equations for the cascaded pi sections shown in Figure 3 produces equations (14) and

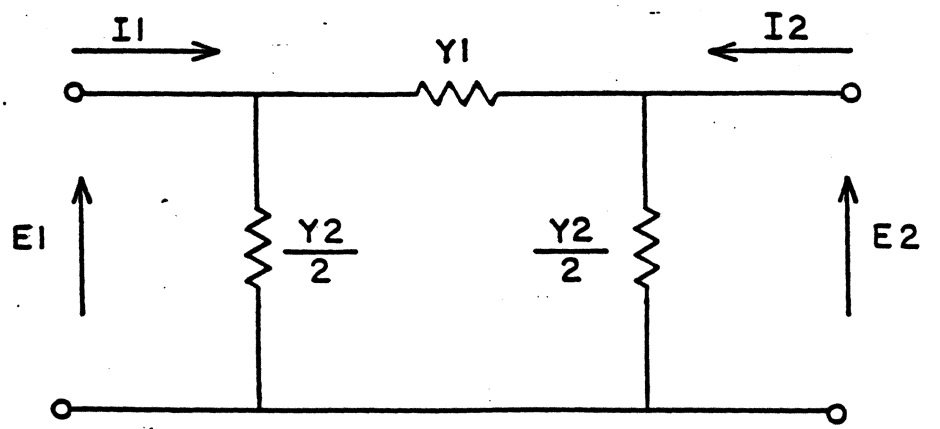

Fig. 2 Single Phase Pi Section

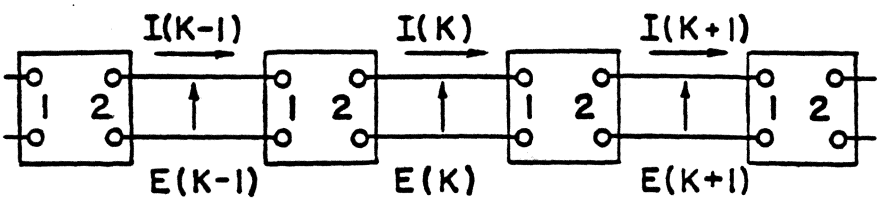

Fig. 3 Single Phase Cascaded Pi Sections

(15).

$$I(k) = -y21 \cdot E(k-1) - y22 \cdot E(k) = y11 \cdot E(k) + y12 \cdot E(k+1) \quad (14)$$

$$E(k) = z21 \cdot I(k-1) - z22 \cdot I(k) = z11 \cdot I(k) - z12 \cdot I(k+1) \quad (15)$$

Equations (14) and (15) can be simplified to (16) and (17).

$$E(k-1) + \frac{2 \cdot y11}{y12} E(k) + E(k+1) = 0 \quad (16)$$

$$I(k-1) - \frac{2 \cdot z11}{z12} I(k) + I(k+1) = 0 \quad (17)$$

Using equation (10) through (13) equation (17) can be written as follows:

$$I(k-1) + \frac{2 \cdot y11}{y12} I(k) + I(k+1) = 0 \quad (18)$$

Equations (16) and (18) are solved by assuming a solution of the following form:

$$E(k) = A\, e^{-K\gamma} \quad (19)$$

$$I(k) = B\, e^{-K\gamma} \quad (20)$$

Substituting (19) and (20) into (16) and (18) produces the following:

$$\left(e^{\gamma} + \frac{2 \cdot y11}{y12} + e^{-\gamma}\right) E(k) = 0 \quad (20)$$

$$\left(e^{\gamma} + \frac{2 \cdot y11}{y12} + e^{-\gamma}\right) I(k) = 0 \quad (21)$$

In solving for γ, the propagation constant of the cascaded pi section, equation (21) simplifies to (22). Using hyperbolic function relations and the impedance relations (8) through (13), produces equation (23).

$$\cosh \gamma = - \frac{y11}{y12} \tag{22}$$

$$\gamma = 2 \sinh^{-1} \sqrt{\frac{Z1}{4 \cdot Z2}} \tag{23}$$

Substituting the boundary conditions E(0) and I(0) into (15), (19) and (20) and simplfying produces (24) the cascaded pi section characteristic impedance.

$$Zc = \frac{A}{B} = z11 - z12 \cdot e^{-\gamma} = \sqrt{\frac{Z1 \cdot Z2}{1 + Z1/(4 \cdot Z2)}} \tag{24}$$

Now consider a single phase line with an impedance (Z), admittance (Y), propagation constant (γ(line)), characteristic impedance (Zc(line)), and length (ℓ) as given in Equations (25) through (28)

$$Z = \ell \cdot (R + j\ L) \tag{25}$$

$$Y = \ell \cdot (G + j\ C) \tag{26}$$

$$\gamma(\text{line}) = \sqrt{Z \cdot Y} \tag{27}$$

$$Zc(\text{line}) = \sqrt{(Z/Y)} \tag{28}$$

To represent this line with cascaded pi sections the values of the impedances of the individual pi section would be as follows:

$$Z1 = Z/n \tag{29}$$

$$1/Z2 = Y/n \tag{30}$$

where Z and Y are the long line impedance and admittance and n is the number of pi sectons used in the representation. Substituting these values (29) and (30) into (23) and (24) and simplifying produces (31) and (32).

$$Zc(pi) = Zc(line)\sqrt{1 + \left(\frac{\gamma(line)}{2n}\right)^2} \tag{31}$$

$$(pi) = 2n \sinh^{-1}\left(\frac{\gamma(line)}{2n}\right) \tag{32}$$

Equations (31) and (32) then relate the error of the characteristic impedance and propagation constant between the long line and the cascaded pi section. The error increases with increasing frequency ($\gamma(line)$ is a function of frequency) and it decreases with increasing n, the number of pi sections. If the square root of equation (31) and the sinh function of equation (32) are expanded in power series, it becomes evident that the error in the characteristic impedance is three times the error in the propagation constant[8].

As an example, consider a line 100 miles long that is modeled with 10 pi sections. At a frequency of 2400 the wavelength would be about 90 miles, and the percent error in $Zc(pi)$ and $\gamma(pi)$ would be 7.9% and 2.6% respectively. In transient analysis problems this frequency response limit on a pi section representation of a line is an important consideration.

IV. CONVERSION TO MODEL COMPONENT VALUES

The line impedance and the charging suseptance matrices output from the EMTP program were used as input to a program which calculated the model component values. This program first scaled the two matrices to model levels. The nominal line voltage and 100 MVA were used as bases for the nominal power system. Model voltages and typical currents were used as the bases for model levels. Reactances were changed to inductances expressed in millihenries, and susceptances were changed to capacitances expressed in microfarads. From these decisions the following scaling factors were established.

$$\text{Resistance factor} = (100\ \text{MVA} / (\text{line KV})^2) \cdot (\text{model voltage} / \text{model current}) \cdot (\text{length}) \tag{33}$$

$$\text{Inductance factor} = (\text{resistance factor}) \cdot (1000 / 377) \tag{34}$$

$$\text{Capacitance factor} = [(\text{line kv})^2 / 100\text{MVA}] \cdot (\text{model current} / \text{model voltage}) \cdot (\text{length}) \cdot (10^6 / 377) \tag{35}$$

Because of the size, weight and the expense involved the total number of inductors must be kept to a minimum. For this reason the same inductors were used in the pi section for each circuit type.

The objective then, in scaling the impedance and susceptance matrices was to produce phase inductances in the impedance matrix which were as closely matched as possible. The model voltage, model base current and line length

represented were the three variables that could be adjusted to produce this. Only two model voltages were used because line sections operating at different voltages must be linked with transformers. More model voltage levels would require more transformers.

Line lengths represented needed to be of a reasonable size. As was shown earlier, each line modeled needs to be composed of several line sections to be represented accurately. If too many line sections were needed to model a line it would prove expensive.

While the inductors were matched as closely as possible, the capacitances and resistances for each voltage level represented were quite different. In the model, these are switched in and out for each voltage level represented. The capacitances that resulted needed to fall in the range of 150 pF to 1 uF. Values smaller than this are difficult to obtain precisely because of stray wiring capacitance and large values tend to be expensive.

The program was run for various combinations of model voltages, currents, and lengths and an acceptable set of base quantities and lengths was decided upon. These decisions are summarized in Table I.

After scaling, the values of the impedance and susceptance matrices became the impedance and susceptance matrices of the pi sections of the model. The equations to

Table I.
Line Section Base Quantities

KV	Circuit Type	Length (Miles)	Voltage (Volts)	Current (Amps)
765	single	50	40	0.025
345	double	7	40	0.025
345	single	10	40	0.025
138	double	20	10	0.100
138	single	20	10	0.100
69	double	4.5	10	0.100
69	single	4.5	10	0.100
34.5	double	1.5	10	0.100
34.5	single	1.4	10	0.100

relate model component values to the matrices were then derived as shown below.

For a single circuit the impedances of the pi section were assumed to have a configuration as shown in Figure 4. The impedance matrix corresponding to this configuration is given by the following:

$$[Z] = \begin{vmatrix} ZA+ZN & ZN+MAB & ZN \\ ZN+MAB & ZB+ZN & ZN+MBC \\ ZN & ZN+MCB & ZC+ZN \end{vmatrix} \qquad (36)$$

If the scaled impedance matrix is represented as follows:

$$[Z] = \begin{vmatrix} Z1 & Z4 & Z5 \\ Z4 & Z2 & Z6 \\ Z5 & Z6 & Z3 \end{vmatrix} \qquad (37)$$

Then when the two matricies are equated the following set of equations (38) results.

$$\begin{aligned} ZN &= Z5 \\ ZA &= Z1 - Z5 \\ ZB &= Z2 - Z5 \\ ZC &= Z3 - Z5 \\ MAB &= Z4 - Z5 \\ MBC &= Z6 - Z5 \end{aligned} \qquad (38)$$

For a double circuit the impedances of the pi section were assumed to have a configuration as shown in Figure 5. The impedance matrix corresponding to this is given by equation (39).

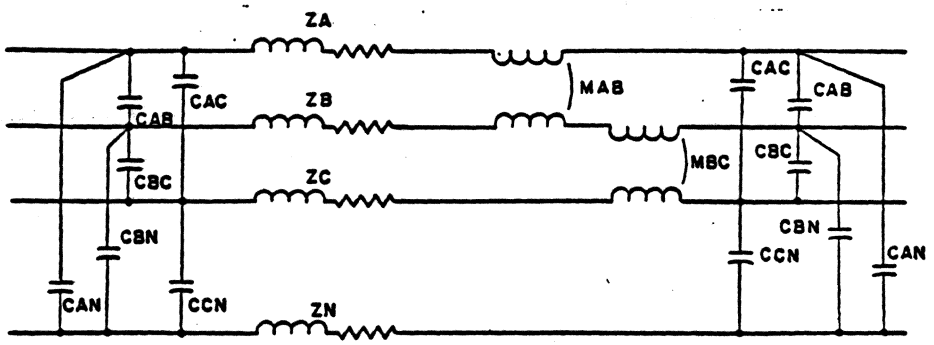

Fig. 4 Single Circuit Configuration

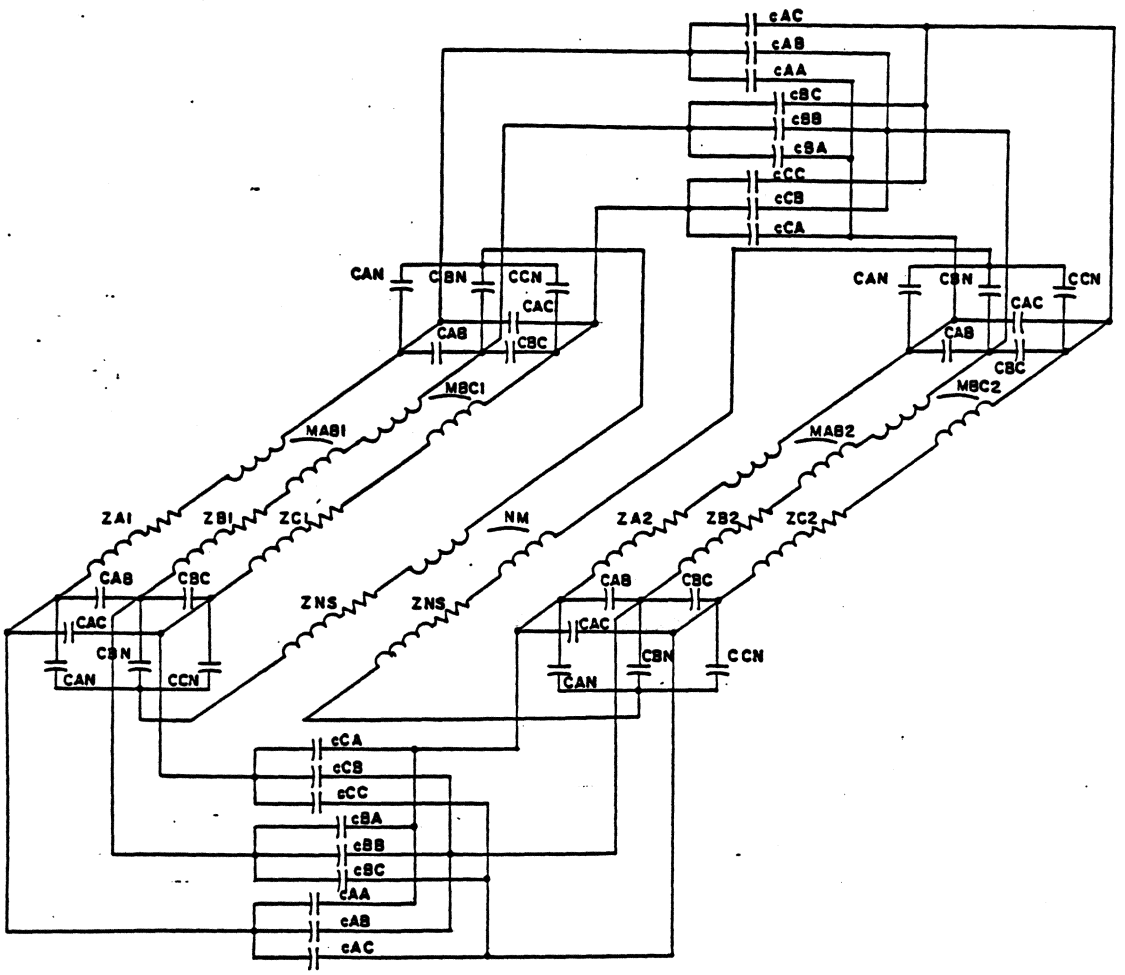

Fig. 5 Double Circuit Configuration

$$[Z] = \begin{vmatrix} ZA1+ZN & MAB1+ZN & ZN & ZN & ZN & ZN \\ MAB1+ZN & ZB1+ZN & MBC+ZN & ZN & ZN & ZN \\ ZN & MBC1+ZN & ZC1+ZN & ZN & ZN & ZN \\ ZN & ZN & ZN & ZA2+ZN & MAB2+ZN & ZN \\ ZN & ZN & ZN & MAB2+ZN & ZB2+ZN & MBC2+ZN \\ ZN & ZN & ZN & ZN & MBC2+ZN & ZC2+ZN \end{vmatrix} \quad (39)$$

where

$$ZN = \frac{ZNS+NM}{2} \quad (40)$$

The scaled matrix is represented as follows.

$$[Z] = \begin{vmatrix} Z1 & Z7 & Z8 & Z13 & Z14 & Z15 \\ Z7 & Z2 & Z9 & Z14 & Z16 & Z17 \\ Z8 & Z9 & Z3 & Z15 & Z17 & Z18 \\ Z13 & Z14 & Z15 & Z4 & Z10 & Z11 \\ Z14 & Z16 & Z17 & Z10 & Z5 & Z12 \\ Z15 & Z17 & Z18 & Z11 & Z12 & Z6 \end{vmatrix} \quad (41)$$

There are now 12 variables in the first case and 18 variables in the second. Since the mutual coupling between circuits is only represented in the neutral in the model, an average of the circuit coupling was used.

$$Z\ (ave) = (Z13 + 2 \cdot Z14 + 2 \cdot Z5 + Z16 + 2 \cdot Z17 + Z18)/9 \quad (42)$$

It was also noted that in all cases Z (ave) was a very good approximation of Z8. This occurs because the spacing between circuits is of the same order as the spacing between A and C phase of each circuit. Equation (41) was then rewritten as follows:

$$[Z] = \begin{vmatrix} Z1 & Z7 & Z8 & Z8 & Z8 & Z8 \\ Z7 & Z2 & Z9 & Z8 & Z8 & Z8 \\ Z8 & Z9 & Z3 & Z8 & Z8 & Z8 \\ Z8 & Z8 & Z8 & Z4 & Z10 & Z8 \\ Z8 & Z8 & Z8 & Z10 & Z5 & Z12 \\ Z8 & Z8 & Z8 & Z8 & Z12 & Z6 \end{vmatrix} \quad (43)$$

Equating (43) and (39) produces the following set of equations.

$$
\begin{aligned}
ZN &= Z8 \\
ZA1 &= Z1-Z8 \\
ZB1 &= Z2-Z8 \\
ZC1 &= Z3-Z8 \\
MAB1 &= Z7-Z8 \\
MBC1 &= Z9-Z8 \\
ZA2 &= Z4-Z8 \\
ZB2 &= Z5-Z8 \\
ZC2 &= Z6-Z8 \\
MAB2 &= Z10-Z8 \\
MAC2 &= Z12-Z8
\end{aligned}
\qquad (44)
$$

This still leaves ZN to be split into ZNS and NM. ZNS was set equal to the single circuit neutral impedance and NM was any remaining inductance.

Equations (38) and (44) now represent self and mutual impedances in the model line section. However, the actual physical mutual inductors will also have a self impedance equal to their mutual impedance. This must be subtracted from the phase self impedances to give component values for the phase self impedances.

Since only a few sizes of inductors were to be built, average values of all the phase and neutral inductors, and all mutual inductors were needed. Average phase inductances, average mutual inductances and average neutral inductances were calculated for each class of lines being modelled (Table II). These average values were then averaged to give the values of the inductors to be used in the model (Table III).

Resistances of the inductor windings were measured and

an estimate of core losses at 60 hertz was made from the manufacturer's curves. These were subtracted from the phase and neutral resistance values to give the resistor sizes needed in each phase and neutral. The higher voltage EHV lines have very high Q's and needed very little resistance added.

The capacitances are calculated in a similar fashion. For a single circuit the susceptances of the pi section were assumed to have a configuration as shown in Figure 4. The capacitance matrix corresponding to this configuration is given by the following:

$$[C] = \begin{vmatrix} CAN+CAB+CAC & -CABZN & -CAC \\ -CAB & CBN+CAB+CBC & -CBC \\ -CAC & -CBC & CCN+CAC+CBC \end{vmatrix} \quad (45)$$

The scaled capacitance matrix is represented by equation (46).

$$[C] = \begin{vmatrix} C1 & C4 & C5 \\ C4 & C2 & C6 \\ C5 & C6 & C3 \end{vmatrix} \quad (46)$$

When the two matricies are equated the following set of equations (47) result.

$$\begin{aligned} CAB &= -0.5 \cdot C4 \\ CAC &= -0.5 \cdot C5 \\ CBC &= -0.5 \cdot C6 \\ CAN &= 0.5 \cdot (C1 + C4 + C5) \\ CBN &= 0.5 \cdot (C2 + C4 + C6) \\ CCN &= 0.5 \cdot (C3 + C5 + C6) \end{aligned} \quad (47)$$

The capacitance derivation for the double circuit is completely analagous to the single circuit case.

The effects of using average inductances in the line

Table II.
Inductance Component Values Calculated

KV	Circuit Type	Average Inductances (mH)			
		Phase		Neutral	
		Self	Mutual	Self	Mutual
765	single	17.5	2.9	10.9	0
345	double	18.0	2.0	7.4	4.1
345	single	20.2	2.8	11.4	0
138	double	20.0	2.3	0	11.0
138	single	22.6	0.8	9.4	0
69	double	18.7	2.1	0	10.3
69	single	18.6	1.7	7.8	0
34.5	double	21.8	2.9	0	19.1
34.5	single	21.7	1.2	18.6	0

Table III.
Inductance Component Values Used In Model

KV	Circuit Type	Average Inductances (mH)			
		Phase		Neutral	
		Self	Mutual	Self	Mutual
765	single	19.5	2.3	10.0	0
345	double	19.5	2.3	0	2.3
345	single	19.5	2.3	10.0	0
138	double	19.5	2.3	0	10.5
138	single	19.5	0	10.0	0
69	double	19.5	2.3	0	10.5
69	single	19.5	2.3	10.0	0
34.5	double	19.5	2.3	0	19.1
34.5	single	19.5	2.3	19.5	0

section must be considered. Changing inductances will affect the propagation matrix and characteristic impedance of the line to be represented. The propagation matrix and characteristic impedance matrix of a multi-phase line are derived from the impedance and admittance matrices as follows [12].

If [L],[R], and [C] are the inductance, resistance, and capcitance matrices for a multi-phase system, then equations (48) and (49) relate the voltage and current in the system.

$$-\frac{\partial[v]}{\partial x} = [L]\frac{\partial[i]}{\partial t} + [R][i] \tag{48}$$

$$-\frac{\partial[i]}{\partial x} = [C]\frac{\partial[v]}{\partial t} \tag{49}$$

Applying the Fourier Transform results in equations that are a function of frequency and changes partial differential equations to ordinary differential equations.

$$-\frac{d[V]}{dx} = [Z(\omega)][I] \tag{50}$$

$$-\frac{d[I]}{dx} = [Y(\omega)][V] \tag{51}$$

where

$$[Z(\omega)] = [R(\omega)] + j\ [L(\omega)]$$
$$[Y(\omega)] = j\ [C(\omega)]$$

When equations (50) and (51) are differentiated with respect to x and proper substitutions are made, the following independent equations, (52) and (53) result.

$$\frac{d^2[V]}{dx^2} = [Z(\omega)][Y(\omega)][V] \tag{52}$$

$$\frac{d^2[I]}{dx^2} = [Y(\omega)][Z(\omega)][I] \tag{53}$$

The following solution is assumed (54 and 55).

$$[V] = e^{-|\lambda_e|x}[A] \tag{54}$$

$$[I] = e^{-|\lambda_i|x}[B] \tag{55}$$

Substituting the assumed solution (54) and (55) into (52) and (53) produces (56) and (57). The differentiation is performed by expanding the exponential function using the Cayley-Hamilton theorem [13] and then differentiating.

$$\frac{d^2[V]}{dx^2} = [\lambda_e]^2[V] \tag{56}$$

$$\frac{d^2[I]}{dx^2} = [\lambda_i]^2[I] \tag{57}$$

Equating (56) and (57) with (52) and (53) yields the following.

$$[\lambda_e] = \{[Z(\omega)][Y(\omega)]\}^{1/2} \tag{58}$$

$$[\lambda_i] = \{[Y(\omega)][Z(\omega)]\}^{1/2} \tag{59}$$

Using the 1st derivative of [I] in (51) produces

$$[\lambda_i][I] = [Y(\omega)][V] \tag{60}$$

$$[V] = [Y(\omega)]^{-1}[\lambda_i][I] \tag{61}$$

$$[V] = [Y(\omega)]^{-1}\{[Y(\omega)][Z(\omega)]\}^{1/2}[I] \tag{62}$$

Equation (62) relating voltage and current at any point along the line defines the characteristic impedance (63).

$$[Zc] = [Y(\omega)]^{-1}\{[Y(\omega)][Z(\omega)]\}^{1/2} \tag{63}$$

Substituting the boundary conditions [V(0)] and [I(0)] into (54) and (55) provides a solution for [A] and [B].

$$[V(o)] = [A] \tag{64}$$
$$[I(o)] = [B] \tag{65}$$

Using average values for the inductors results in a change in the propagation matrix for the line section. The propagation matrix must remain constant in order for the line section to continue to represent the same length of line. To maintain the same propagation matrix, the LC product (for the lossless line) must remain the same. A new capacitance matrix is calculated to maintain this product.

$$[C'] = [L']^{-1} \; [L][C] \tag{66}$$

where

[C'] = New capacitance matrix
[L'] = New inductance matrix (with average inductances)
[L] = Original inductance matrix
[C] = Original capacitance matrix

For the lossless case, the new characteristic impedance matrix of the line section is now

$$[Zc'] = [C']^{-1}\{[C'][L']\}^{1/2} \tag{67}$$

V. MODEL DESIGN

After averaging the inductance values, five inductors were selected to be built. The cores selected are manufactured by Arnold Engineering, Marengo, Illinois. The cores are made from a oriented alloy of 50% nickel and 50% iron. It has a saturation flux density of 1.5 Tesla. Single winding inductors were wound on 4 mil cores. The two winding mutual inductors were wound on 2 mil cores which have a lower core loss than the 4 mil cores. These cores have a very square magnetization curve[6] as in Figure 6. They have relatively low losses (approximately 0.2 watts per pound at 60 Hertz).

There were several constraints involved in the inductor design. The air gap length in the core had to be large enough to be able to control it precisely but small enough to prevent a large fringing flux. This limited the air gap to the range of 0.7 to 10 millimeters. Another constraint was that the Q of the coil must be high. The higher voltage lines have higher Q's than the lower voltage lines. Number 12 wire was used so that the resistance of the windings could be kept low, resulting in a higher Q. The lower Q's for lower voltage lines were obtained by inserting a resistor in series with the inductor.

Finally, the inductor could not go into saturation at short circuit current levels. A value of 5 amps was used

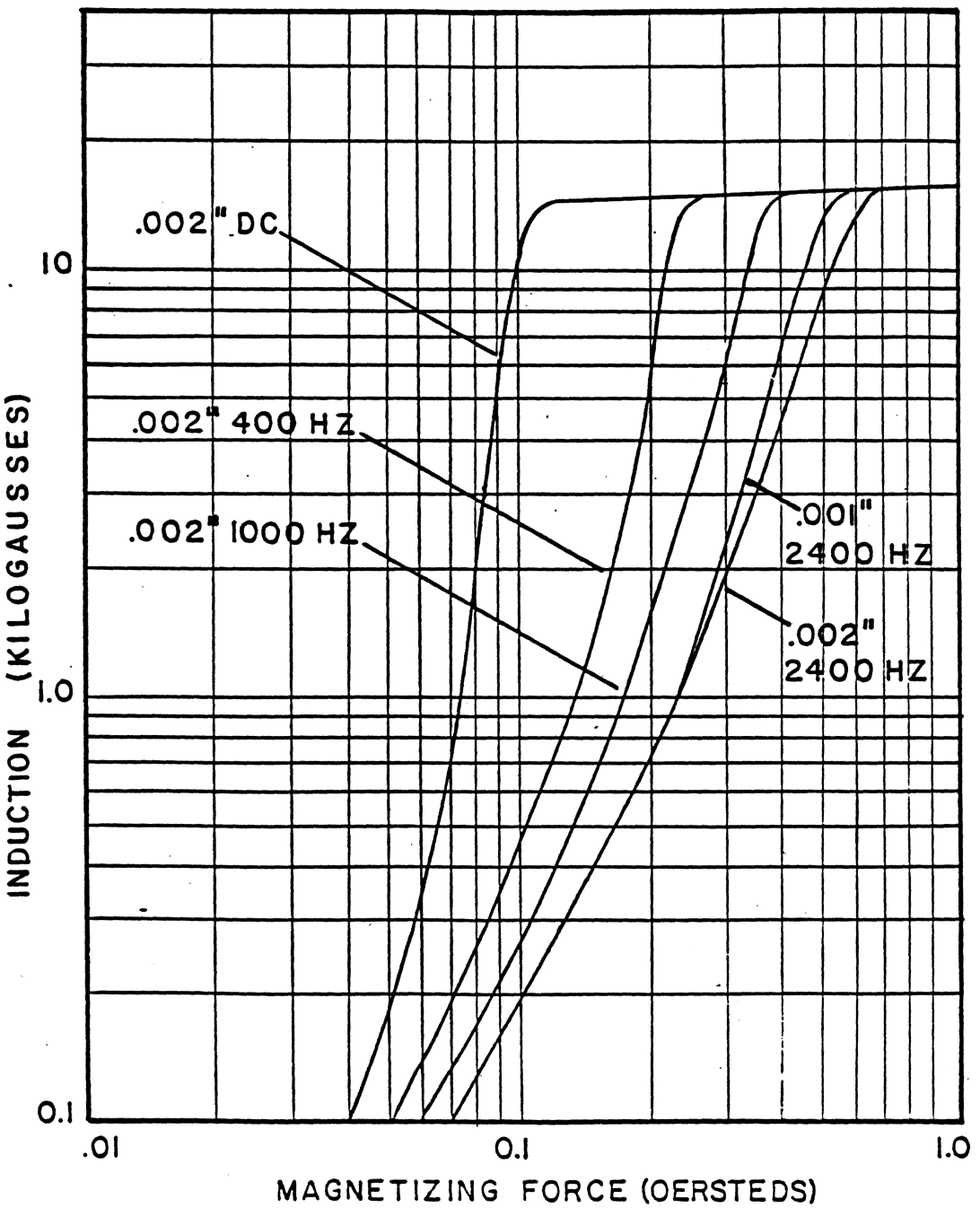

Fig. 6 Magnetization Curve

for the inductor design.

The following equations (70) and (71) relate core dimensions and currents with inductances and magnetic flux densities.

$$L = \frac{0.4 \cdot \pi \cdot N^2 \cdot A \cdot 10^8}{lg + l/\mu m} \tag{68}$$

$$Bmax = \frac{0.4 \cdot \pi \cdot N \cdot I \cdot 10^8}{lg + l/\mu m} \tag{69}$$

where

L = inductance in henries
N = number of turns
A = cross sectional area of iron core in cm
I = RMS current in amperes
Bmax = maximum flux density in teslas
lg = gap length in centimeters
l = mean length of iron core
μm = permeability of iron core

For the gap lengths and core dimensions used in these inductors these equations reduce to the given by equations (70 and 71).

$$L = \frac{0.4 \cdot \pi \cdot N^2 \cdot A \cdot 10^8}{lg} \tag{70}$$

$$Bmax = \frac{0.4 \cdot \pi \cdot N \cdot I \cdot 10^8}{lg} \tag{71}$$

Using an average value for gap length and 5 amps for the current, a trial and error approach was used to select a core of approximately the right dimension. Core dimensions affect the number of turns and the cross sectional area of

the core. The inductor was then designed by adjusting the number of turns and the gap length. An acceptable design was one in which the coil filled the window area of the coil, the gap was within the right range, and the inductor did not saturate at high current levels.

All components for the model were selected to maintain a two percent accuracy in the model. All but the .51 ohm resistors were three watt, one percent tolerance resistors. The .51 ohm resistors were five percent, two watt resistors.

The capacitors that were used had varying tolernces from one percent to ten percent. However, the capacitance of all the capacitors was measured to maintain the two percent accuracy. The smaller capacitors, up to 1500 pF have a 500 volt rating. From 1800 pF to .33 uF the capacitors have a 600 volt rating and the .47 uF and above have a 400 volt rating.

In building the pi sections two types (designated type 1 and type 2) of chassis were used. The type 1 contains the double circuit coupling capacitors, the extra switch for these capacitors and the neutral mutual inductors which are used in the double circuit representation. Separate chassis were also used for HV and EHV line sections. This results in four different type chassis being built.

Figures 7 through 16 provide a view of the mechanical design of the pi sections. Figures 17 through 20 show the electrical connections of each of the four types of pi

sections. All values on figures 17 through 20 are calculated values. Resistances are in ohms, inductances are in millihenries, and capacitances are in picofarads and microfarads. Figures 21 and 22 show pictures of the front panel and chassis internals of the HV type 1 chassis.

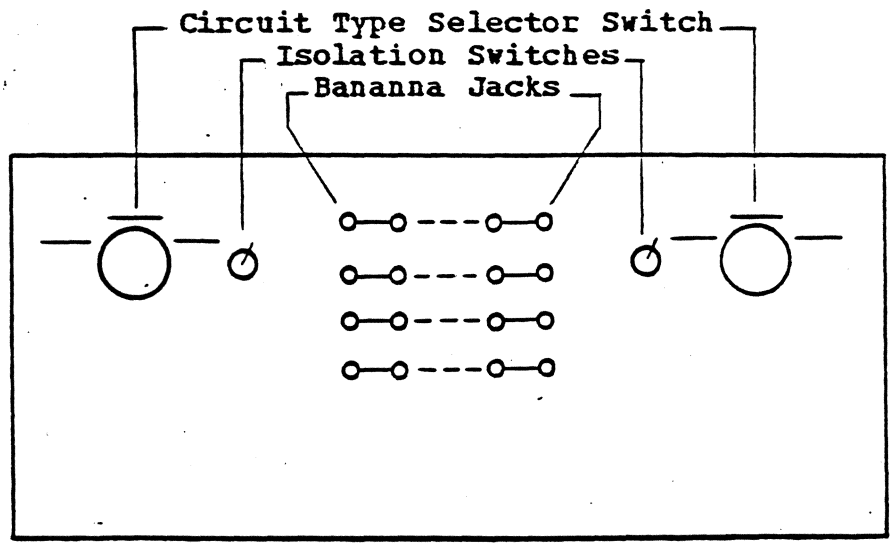

Fig. 7 Chassis 1 Front Panel Layout

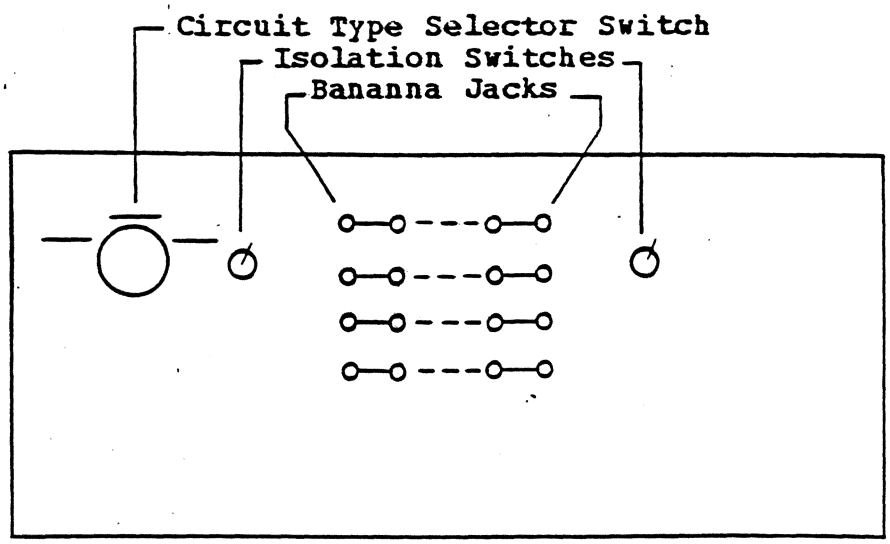

Fig. 8 Chassis 2 Front Panel Layout

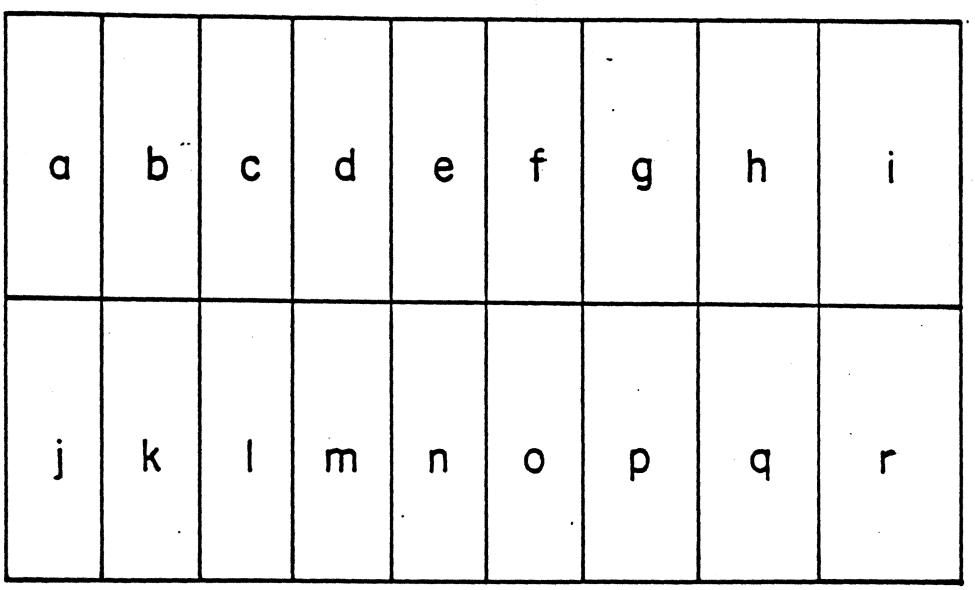

a. 34.5 kv, 1 ckt, side 1
b. 34.5 kv, 1 ckt, side 2
c. 69 kv, 1 ckt, side 1
d. 69 kv, 1 ckt, side 1
e. 138 kv, 1 ckt, side 1
f. 138 kv, 1 ckt, side 2
g. 138 kv, coup., side 1
h. 34.5 kv, coup., side 1
i. 34.5kv, coup., side 2
j. 34.5 kv, 2 ckt, side 1
k. 34.5 kv, 2 ckt, side 2
l. 69 kv, 2 ckt, side 1
m. 69 kv, 2 ckt, side 2
n. 138 kv, 2 ckt, side 1
o. 138 kv, 2 ckt, side 2
p. 138 kv, coup., side 2
q. 69 kv, coup., side 1
r. 69 kv, coup., side 2

Fig. 9 HV Chassis 1 Capacitor Board Layout

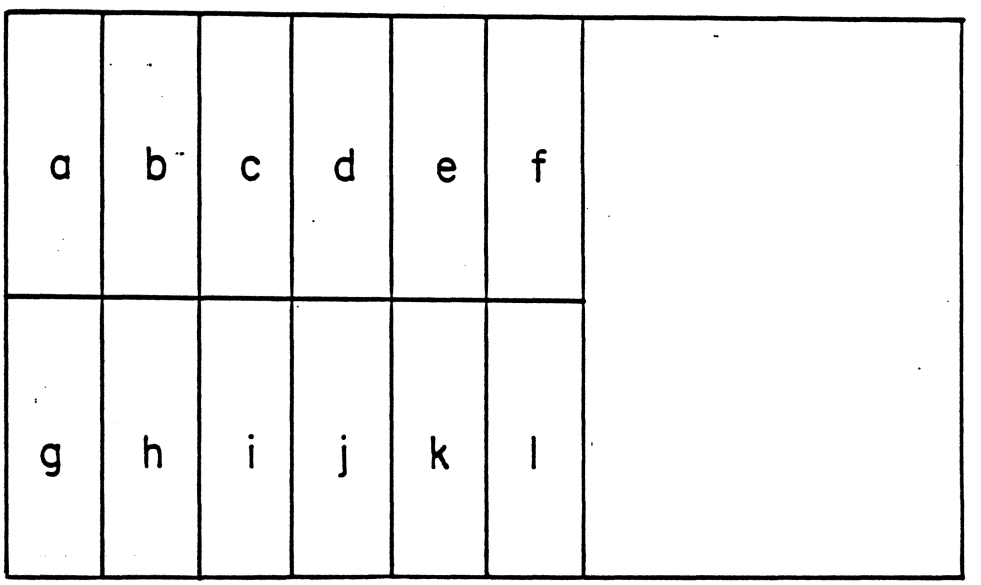

a. 34.5 kv, 1 ckt, side 1
b. 34.5 kv, 1 ckt, side 2
c. 69 kv, 1 ckt, side 1
d. 69 kv, 1 ckt, side 1
e. 138 kv, 1 ckt, side 1
f. 138 kv, 1 ckt, side 2
g. 34.5 kv, 2 ckt, side 1
h. 34.5 kv, 2 ckt, side 2
i. 69 kv, 2 ckt, side 1
j. 69 kv, 2 ckt, side 2
k. 138 kv, 2 ckt, side 1
l. 138 kv, 2 ckt, side 2

Fig. 10 HV Chassis 2 Capacitor Board Layout

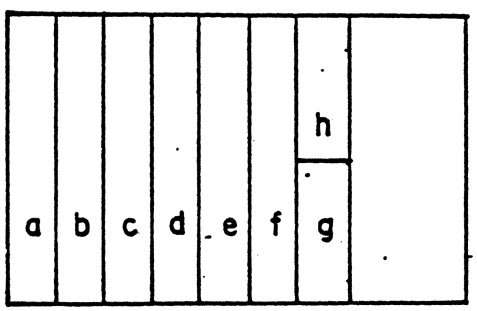

a. 765 kv, 1 ckt, side 1
b. 765 kv, 1 ckt, side 2
c. 345 kv, 2 ckt, side 1
d. 345 kv, 2 ckt, side 2
e. 345 kv, 1 ckt, side 1
f. 345 kv, 1 ckt, side 2
g. 345 kv, coup., side 1
h. 345 kv, coup., side 2

Fig. 11 EHV Chassis 1 Capacitor Board Layout

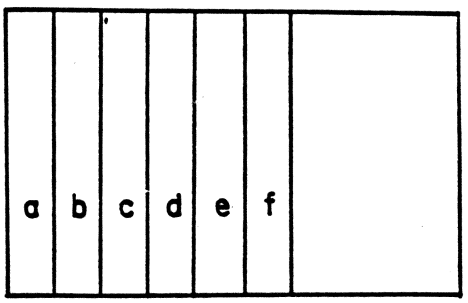

a. 765 kv, 1 ckt, side 1
b. 765 kv, 1 ckt, side 2
c. 345 kv, 2 ckt, side 1
d. 345 kv, 2 ckt, side 2
e. 345 kv, 1 ckt, side 1
f. 345 kv, 1 ckt, side 2

Fig. 12 EHV Chassis 2 Capacitor Board Layout

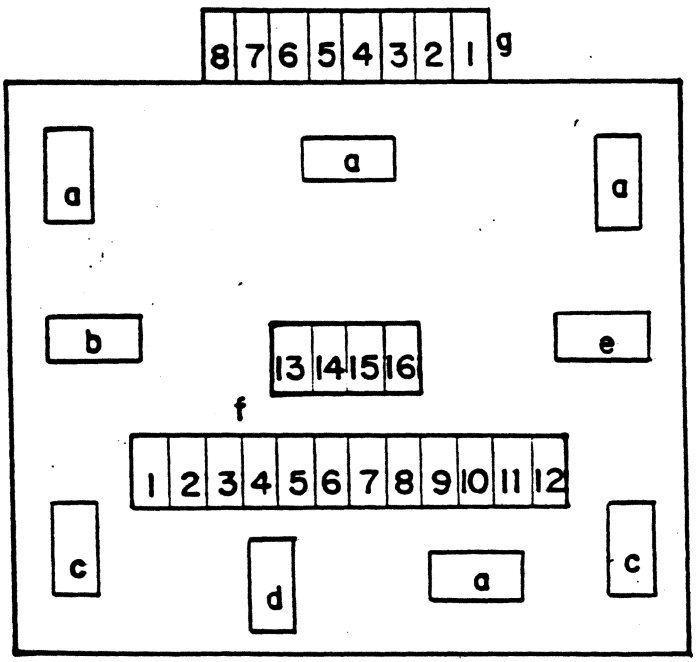

a. 19.5 mH
b. 10.5 mH
c. 2.3 mH
d. 10.0 mH
e. 19.1 mH
f. Terminal block 1
g. Terminal block 2

Fig. 13 HV Chassis 1 Layout

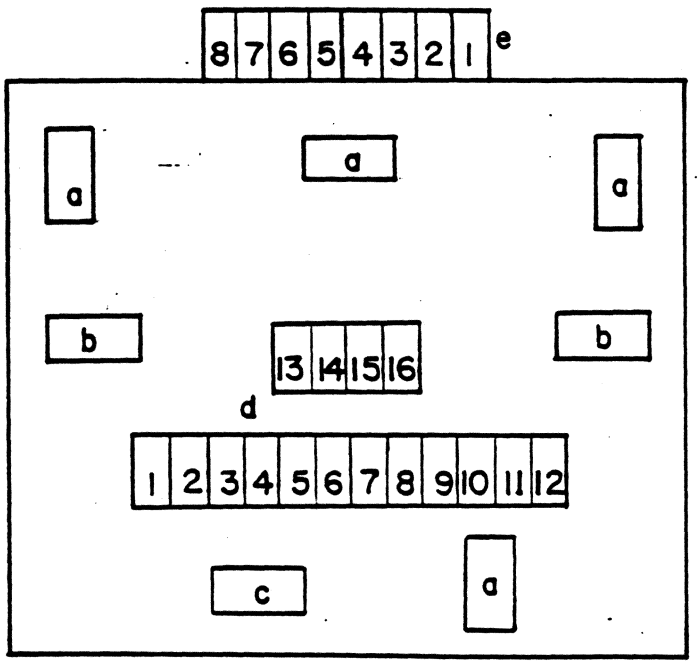

a. 19.5 mH
b. 2.3 mH
c. 10.0 mH
d. Terminal block 3
e. Terminal block 4

Fig. 14 HV Chassis 2 Layout

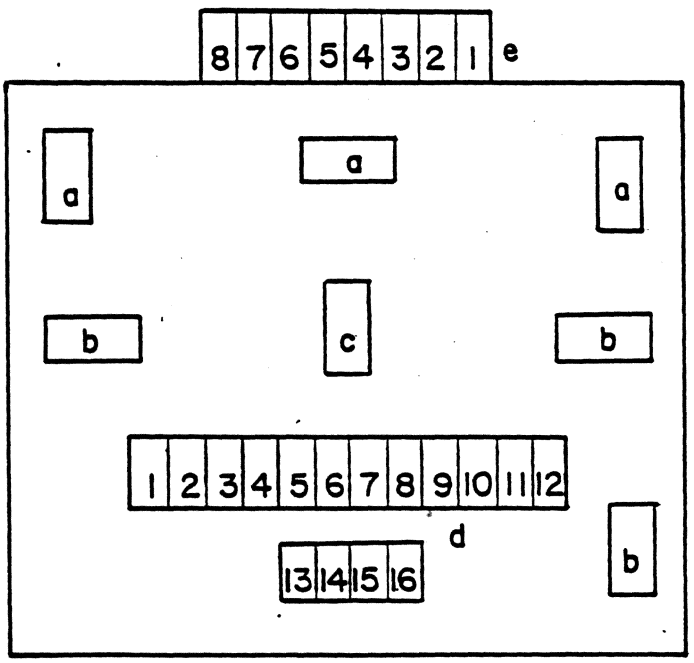

a. 19.5 mH
b. 2.3 mH
c. 10.0 mH
d. Terminal block 1
e. Terminal block 2

Fig. 15 EHV Chassis 1 Layout

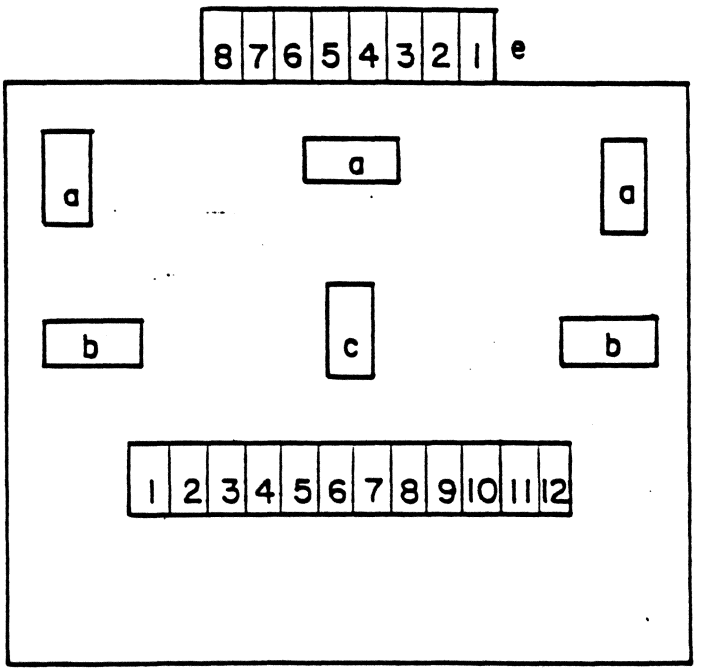

a. 19.5 mH
b. 2.3 mH
c. 10.0 mH
d. Terminal block 3
e. Terminal block 4

Fig. 16 EHV Chassis 2 Layout

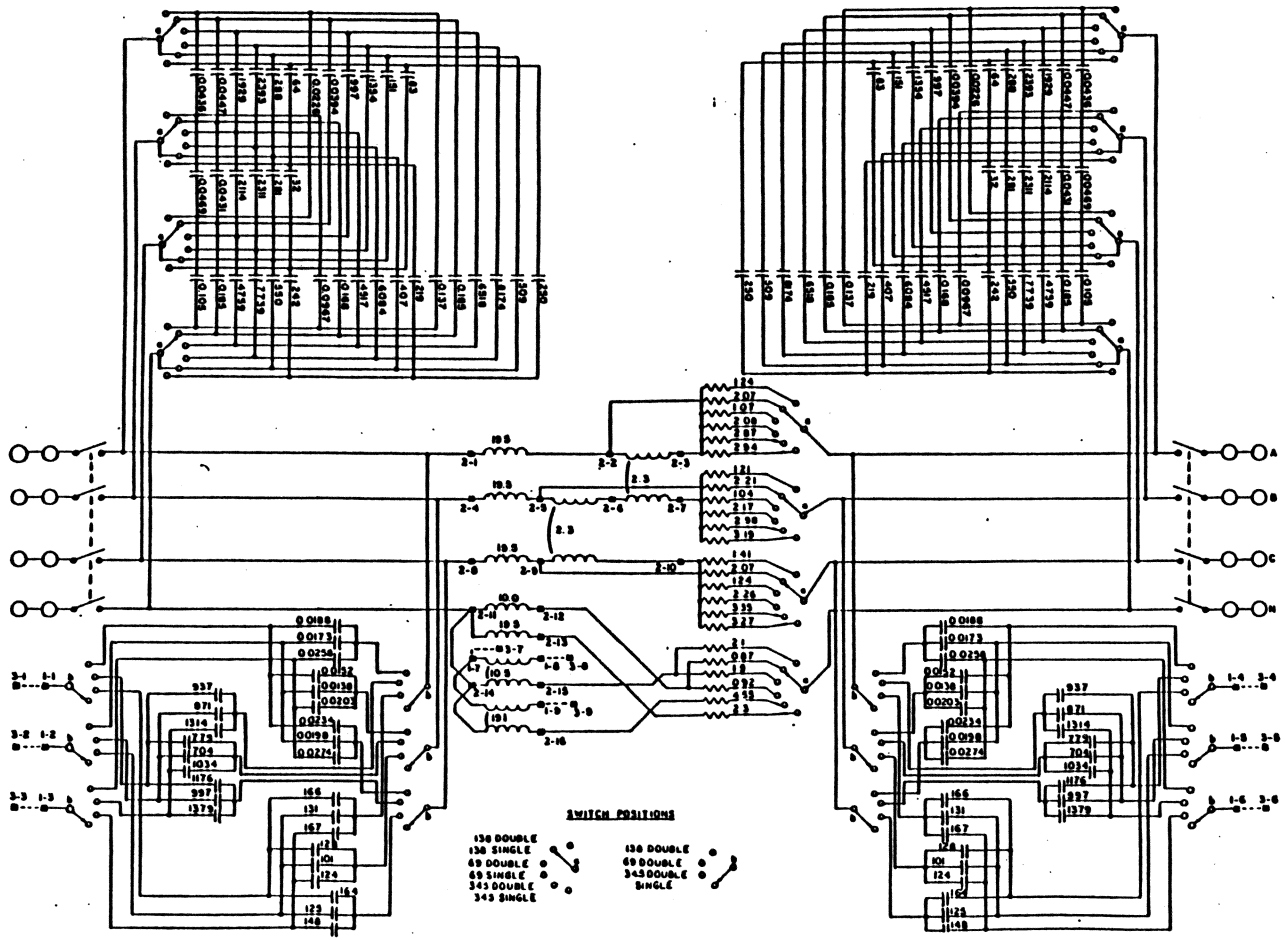

Fig. 17 HV Chassis 1 Schematic

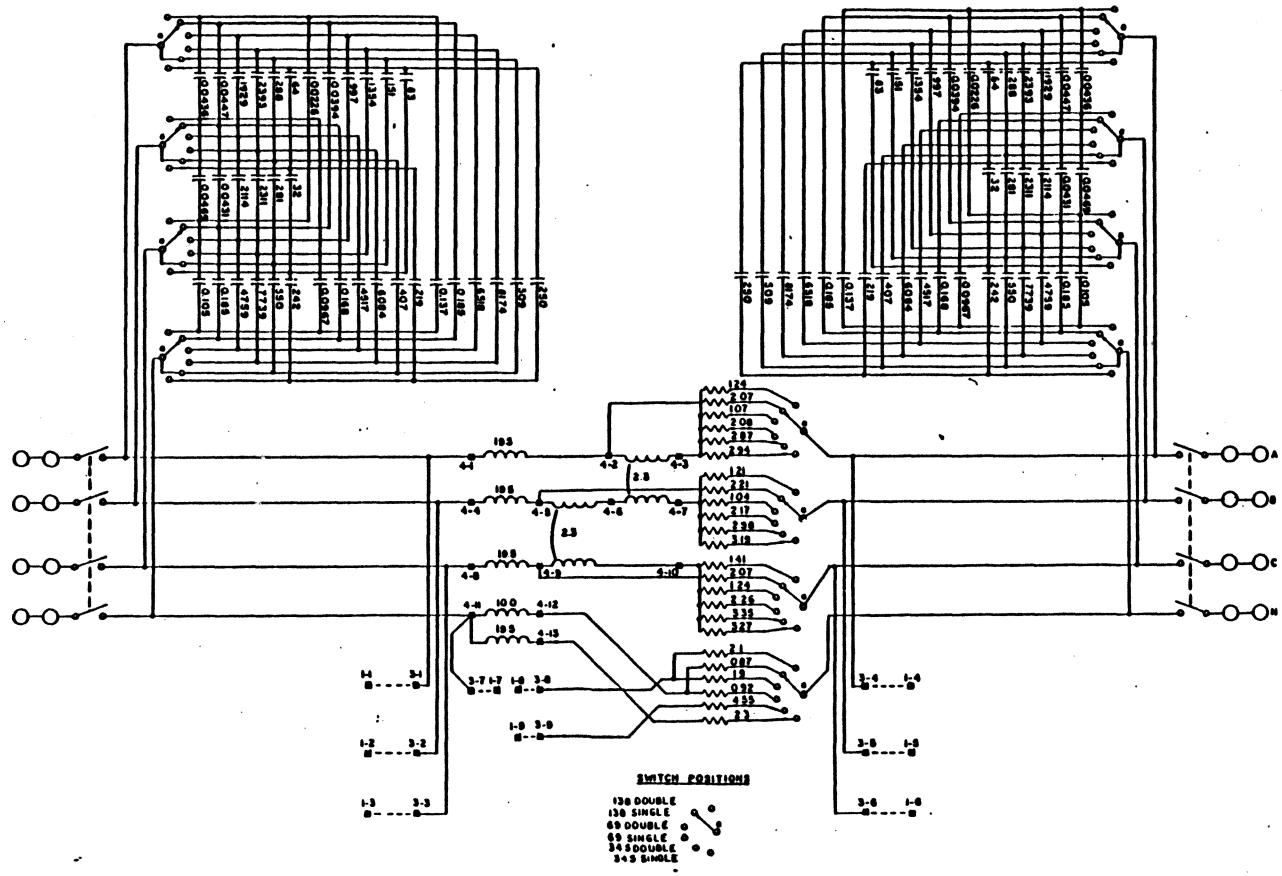

Fig. 18 HV Chassis 2 Schematic

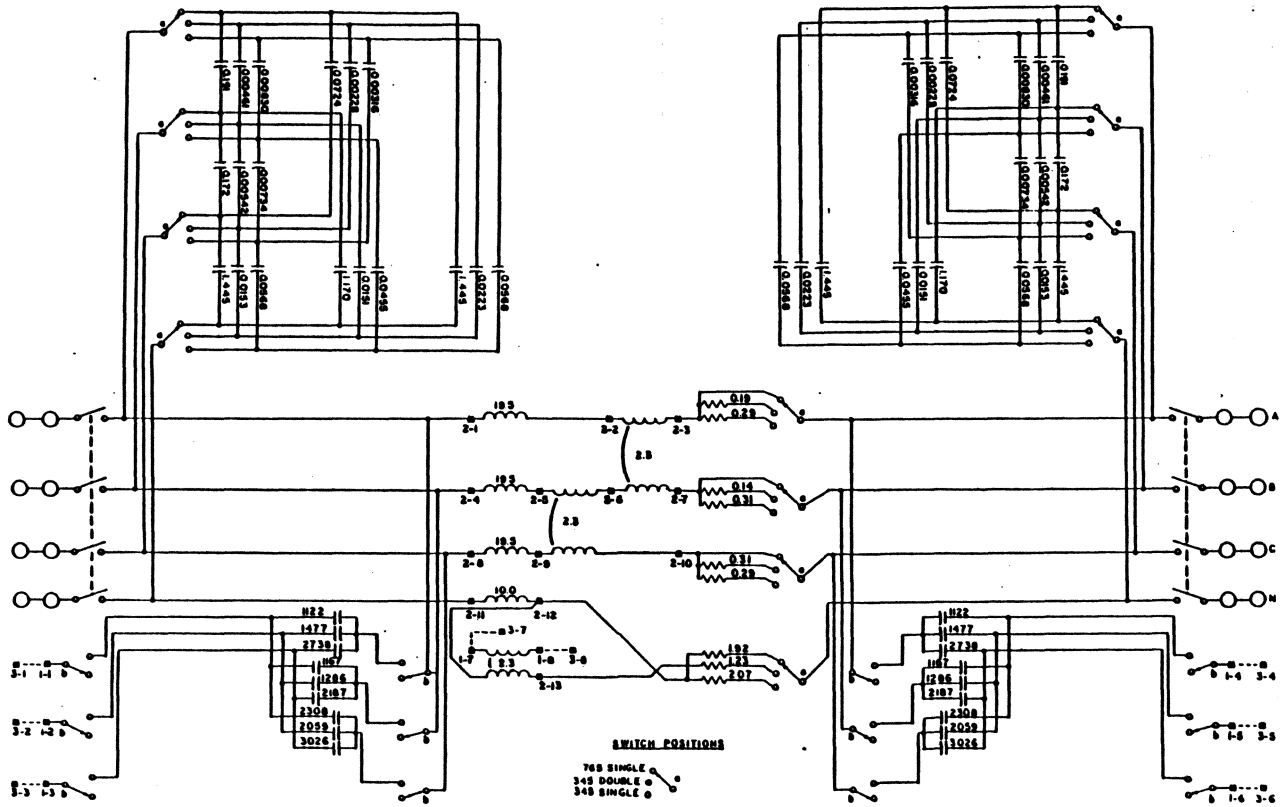

Fig. 19 EHV Chassis 1 Schematic

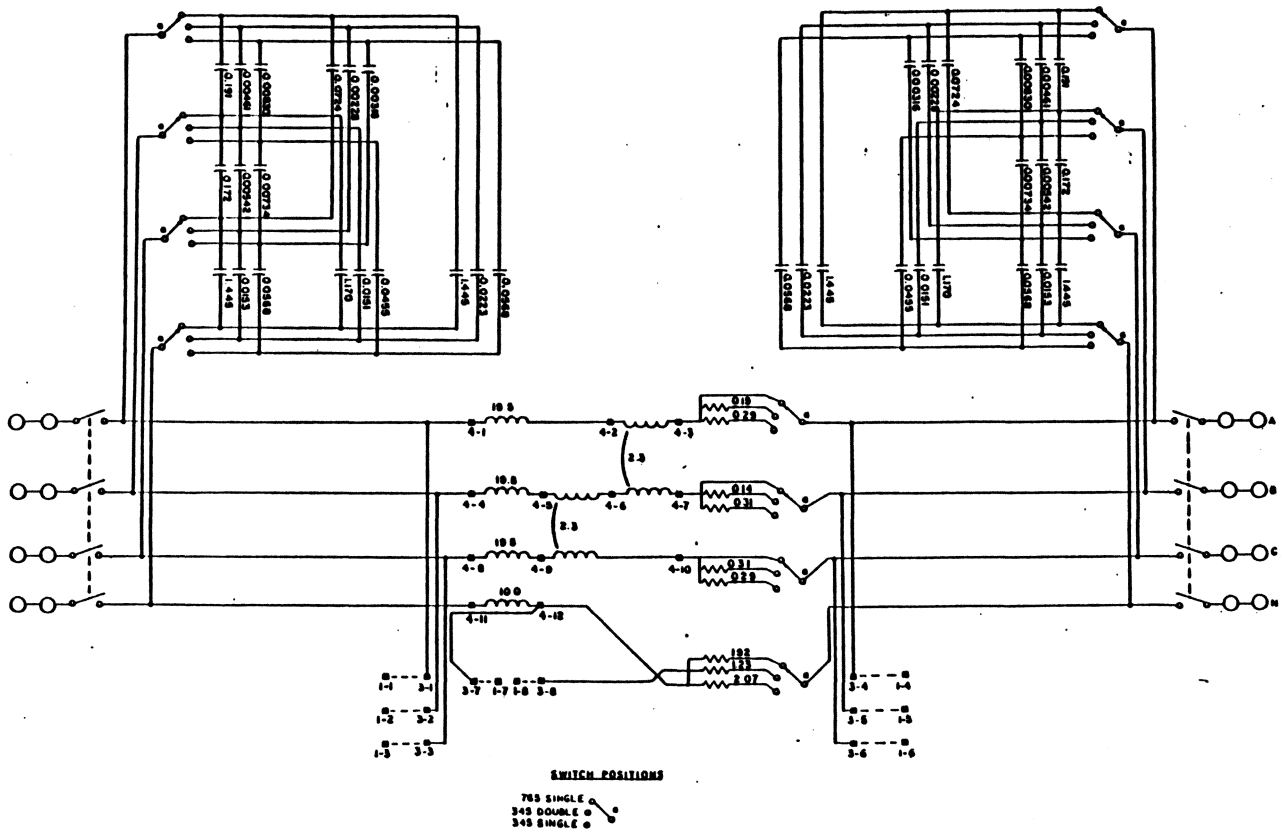

Fig. 20 EHV Chassis Schematic

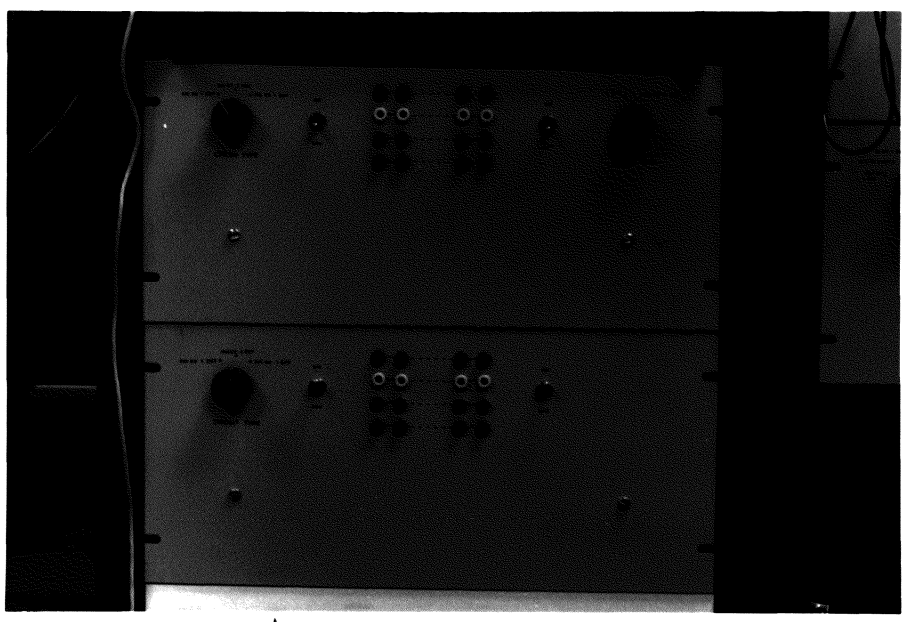

Fig. 21 EHV Type 1 and 2 Chassis Front Panel

Fig. 22 EHV Type 1 Chassis Internals

VI. MODEL TESTING

The testing involved tests of the inductors and tests of the complete pi section. Both steady state and transient tests were performed. Initial inductor checks were made by measuring voltages and phase angles across a resistor placed in series with the inductor. These tests indicated that inductances were within three percent of design values at 60 hertz. Further testing was done on the 19.5, 10.0, and 2.3 mH. inductors. Pictures (Figure 21) of the oscilliscope trace were made as a capacitor (3.105 microfarads) was discharged through the inductor. From the frequency of oscillation, the inductor sizes were then calculated. From the decay rate, the inductor resistance was calculated. These results are shown in Table IV.

Steady state values of open circuit voltages and short circuit currents were calculted for each pi section. These quantities were then measured and compared to the calculated values. All tests were made with 10 volt inputs. The voltages were generated by a real time computer based generator model. The frequency of this voltage source was 59.9 hertz. For the open circuit test, voltage was applied to phase 'A' and the voltage on the other phases were measured. For the short circuits, 10 volt balanced three phase voltages were applied to one end of the section and currents were measured on the phases indicated in the table.

These results are shown in Tables V through IX. Values

measured in the 34.5 KV open circuit tests floated up and down about five percent each way. Values shown in the tables are averages for these floating voltages.

Transient response to a 10 volt step wave was measured. Two 138 KV single circuit sections were connected in series for the transient test. Figure 24 shows the receiving end voltage for the positive sequence mode. The time scale is one milliseconds per division. Figure 25 shows the receiving end voltage for the zero sequence mode. The time scale is one milliseconds per division. From these the velocities of propagation were calculated to be 181,000 miles per second for the positive sequence and 124,000 miles per second for the zero sequence. Neither trace shows a square wave response because of the limited frequency response obtained by using only two sections.

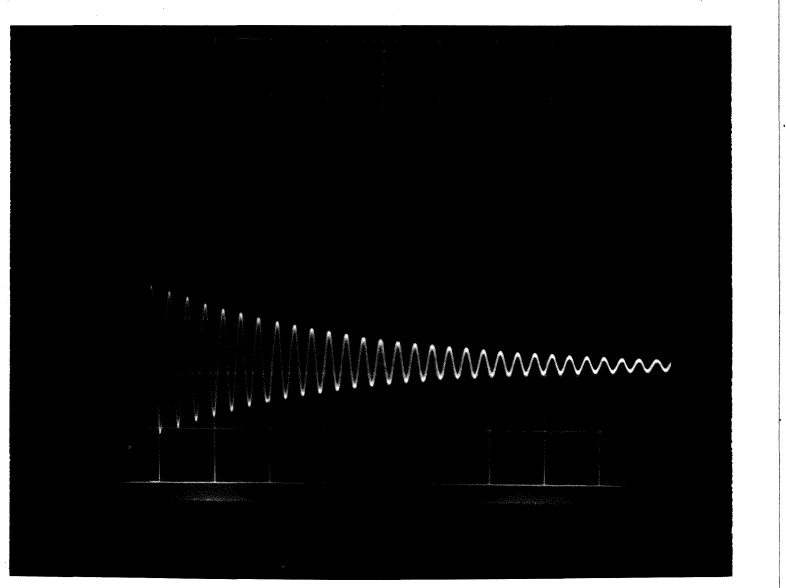

Fig. 23 Capacitor Discharge Through 19.5 mH Inductor

Table IV.
Inductor Test Results

Inductor (mH)	Oscillation Frequency (Hz)	Measured Inductance (mH)	Inductance Error (%)	Measured Resistance (Ohms)
19.5	634.4	20.27	3.9	1.1
10.0	891.7	10.26	2.6	2.0
2.3	1860	2.36	2.5	2.1

Table V.
EHV Open Circuit Test Results

KV	Circuit Type	Phase	Chassis	Calculated (Volts)	Measured (Volts)	Error (%)
765	Single	A	1	10.0	10.0	0.
		B	1	1.30	1.32	1.5
		C	1	0.561	0.55	2.0
345	Double	A	1	10.0	10.0	0.
		B	1	1.96	1.98	1.0
		C	1	1.35	1.38	2.2
		A	2	0.716	0.73	2.0
		B	2	1.03	1.03	0.
		C	2	1.39	1.39	0.
345	Single	A	1	10.0	10.0	0.
		B	1	1.41	1.43	1.4
		C	1	0.625	0.63	0.8

Table VI.
HV Open Circuit Test Results

KV	Circuit Type	Phase	Chassis	Calculated (Volts)	Measured (Volts)	Error (%)
138	Double	A	1	10.0	10.01	0.
		B	1	2.57	2.58	0.4
		C	1	1.90	1.90	0.
		A	2	1.48	1.47	0.7
		B	2	1.68	1.68	0.
		C	2	1.91	1.91	0.
138	Single	A	1	10.0	10.0	0.
		B	1	2.05	2.05	0.
		C	1	1.80	1.81	0.6
69	Double	A	1	10.0	10.0	0.
		B	1	2.57	2.57	0.
		C	1	1.90	1.91	0.5
		A	2	1.46	1.45	0.7
		B	2	1.67	1.65	1.2
		C	2	1.92	1.90	1.1
69	Single	A	1	10.0	10.0	0.
		B	1	2.66	2.67	0.3
		C	1	1.77	1.77	0.
34.5	Double	A	1	10.0	10.0	0.
		B	1	3.38	3.29	2.7
		C	1	2.52	2.48	1.6
		A	2	2.59	2.40	7.3
		B	2	2.57	2.35	8.6
		C	2	2.53	2.33	7.9
34.5	Single	A	1	10.0	10.0	0.
		B	1	3.32	3.22	3.0
		C	1	2.52	2.46	2.4

Table VII.
Phase A to Ground Short Circuit Test Results

KV	Circuit Type	Phase	Chassis	Calculated (Amps)	Measured (Amps)	Error (%)
765	Single	A	1	0.815	0.810	0.6
			2		0.810	0.6
345	Double	A	1	0.904	0.909	0.5
			2		0.909	0.5
345	Single	A	1	0.809	0.802	0.9
			2		0.787	2.7
138	Double	A	1	0.801	0.794	0.9
			2		0.794	0.9
138	Single	A	1	0.857	0.840	2.0
			2		0.843	1.6
69	Double	A	1	0.804	0.797	0.9
			2		0.798	0.7
34.5	Double	A	1	0.607	0.598	1.5
			2		0.599	1.3
34.5	Single	A	1	0.600	0.593	1.2
			2		0.595	0.8

Table VIII.
Line to Line to Ground Short Circuit Test Results

KV	Circuit Type	Chassis	Phase	Calculated (Amps)	Measured (Amps)	Error (%)
765	Single	1	A	1.111	1.098	3.0
			B	1.179	1.126	4.5
		2	A	1.111	1.097	1.3
			B	1.179	1.170	0.76
345	Double	1	A	1.174	1.144	2.6
			B	1.141	1.109	2.8
		2	A	1.174	1.159	1.3
			B	1.141	1.133	0.70
	Single	1	A	1.110	1.080	2.7
			B	1.173	1.130	3.7
		2	A	1.110	1.064	4.1
			B	1.173	1.179	0.51
138	Double	1	A	1.150	1.195	3.9
			B	1.094	1.050	4.0
		2	A	1.150	1.119	2.7
			B	1.094	1.069	2.3
	Single	1	A	1.168	1.130	3.3
			B	1.163	1.120	3.7
		2	A	1.168	1.149	1.6
			B	1.163	1.141	1.9
69	Double	1	A	1.155	1.098	4.9
			B	1.099	1.052	4.3
		2	A	1.115	1.124	2.7
			B	1.099	1.072	2.5
	Single	1	A	1.133	1.070	5.6
			B	1.055	1.003	4.9
		2	A	1.133	1.097	3.2
			B	1.055	1.020	3.3
34.5	Double	1	A	1.069	1.012	4.9
			B	0.999	0.942	4.1
		2	A	1.069	1.033	2.8
			B	0.999	0.959	2.3
	Single	1	A	1.069	1.012	5.3
			B	0.999	0.942	5.7
		2	A	1.069	1.033	3.4
			B	0.999	0.959	4.0

Table IX.
3 Phase to Ground Short Circuit Test Results

KV	Circuit Type	Chassis	Phase	Calculated (Amps)	Measured (Amps)	Error (%)
765	Single	1	A	1.265	1.252	1.0
			B	1.279	1.215	5.0
			C	1.252	1.220	2.6
345	Double	1	A	1.272	1.246	2.0
			B	1.267	1.218	3.9
			C	1.251	1.227	1.9
	Single	1	A	1.263	1.247	1.3
			B	1.276	1.217	4.6
			C	1.247	1.220	2.2
138	Double	1	A	1.250	1.191	4.7
			B	1.246	1.197	3.9
			C	1.216	1.182	2.8
	Single	1	A	1.291	1.224	3.6
			B	1.292	1.262	2.3
			C	1.297	1.260	2.9
69	Double	1	A	1.254	1.200	4.3
			B	1.252	1.196	4.5
			C	1.223	1.193	2.5
	Single	1	A	1.221	1.159	5.1
			B	1.209	1.153	4.6
			C	1.183	1.144	3.3
34.5	Double	1	A	1.174	1.114	5.1
			B	1.167	1.123	3.8
			C	1.128	1.084	3.9
	Single	1	A	1.170	1.112	5.0
			B	1.168	1.107	5.2
			C	1.132	1.081	4.5

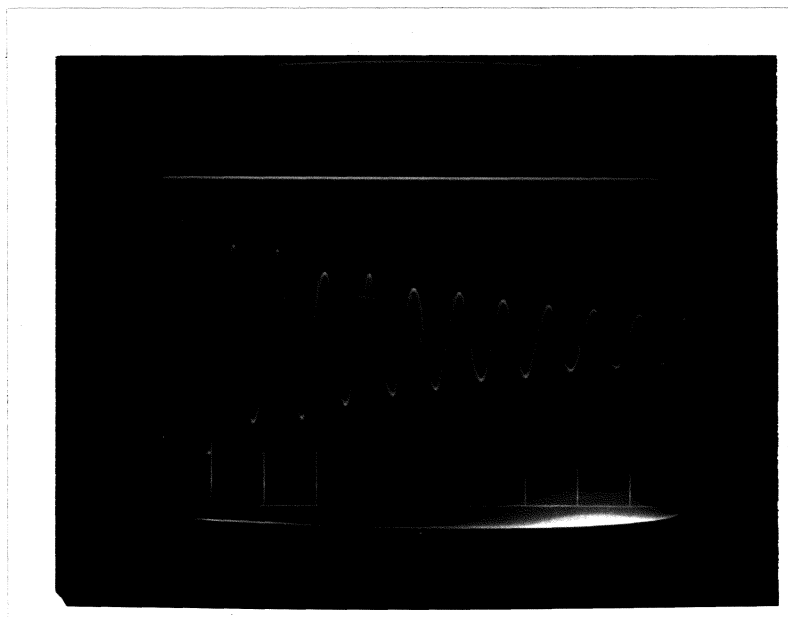

Figure 24 Positive Sequence Propagation Mode

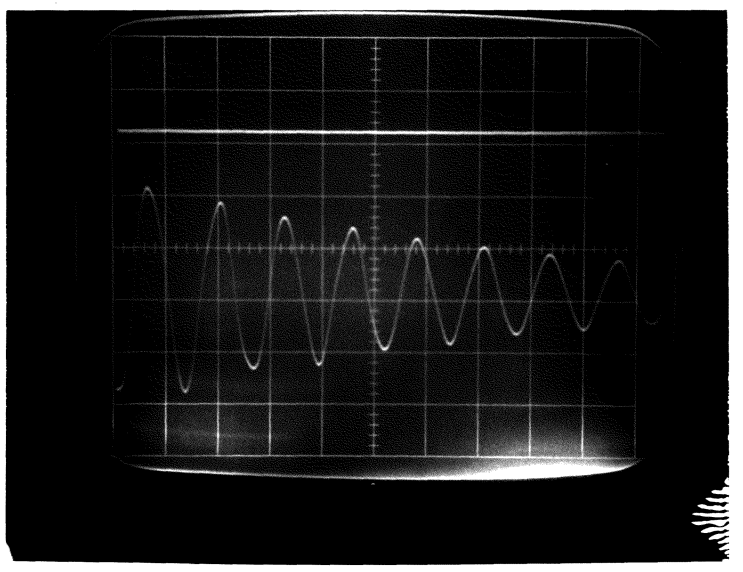

Figure 25 Zero Sequence Propagation Mode

V. CONCLUSIONS

Inductor resistances shown in Table IV are much higher than those estimated from the manufactures curves at 60 hertz (Appendix). Estimates from the manufactures curves at the frequencies of oscillation agree with the resistances as measured in Table IV. This means that the resistances in the model are very frequency dependent.

In the steady state, all values except the 34.5 kv open circuit voltages are accurate to 5.2 percent. Test results indicate that the floating voltages measured on the 34.5 kv open circuit test result from stray capacitances which affect the small (125 picofarads) values used in the model.

All but two of the short circuit currents measured were lower than the calculated values. Further study is needed to determine if this is caused by greater core losses than expected or by inductors that are larger than design values.

The distortion of the waveforms (from the expected square waves) in the transient response test result from using only two sections. The propagation velocities measured are appropriate for the line modeled.

VII. REFERENCES

1. W.S. Meyer and H.W. Dommel, "Numerical Modeling of Frequency-Dependent Transmission-line Parameters in an Electromagnetic Transients Program", IEEE Trans. Power Apparatus and Systems, vol. PAS-93, pp. 1401-1409, Sept/Oct. 1974.

2. H.W. Dommel, "Digital Computer Solutin of Electromagnetic Transients in Single and Multi-phase Networks." IEEE Trans. Power Apparatus and Systems, vol. PAS-88, pp.388-399, April 1969.

3. "Silectron Cores", Bulletin SC-107B, Arnold Engineering, Marengo, Ill.

4. "Cut Core Design Manual", Catalog No. SC-142A, Arnold Engineering, Marengo, Ill.

5. J.R. Carson, "Wave propagation in overhead wires with ground return", Bell System Technical Journal, vol. 5, pp. 539-554, 1926

6. "Tape Wound Cores", Bulletin TC-101C, Arnold Engineering, Marengo, Ill.

7. Stevenson, Jr., William D., Elements of Power System Analysis, 3rd edition, McGraw-Hill Inc., New York, 1975.

8. Guillemin, Ernst A., Communications Networks, Vol II, John Wiley and Sons, Inc., New York, 1935

9. J. K. Dickson, D. E. Hedman, W. A. Lewis, R. M. Webler, "A New TNA - Part 1 - Design Features Provide Versatile Capabilities", IEEE PES Summer Power Meeting, 1973.

10. K. Carlson, D. P. Carroll, G. E. Gareis. P. C. Krause, F. Nozari, C. M. Ong, D. M. Triczenberg, "Design of a Power System Simulator", IEEE PES Winter Meeting, 1978.

11. W. S. Meyer and T. H. Liu, Eds., "Electromagnetic Transients Program Rule Book", Portland Oregon: Bonnevile Power Administration, 1980, 750 pages.

12. D. E. Hedman," Propagation on Overhead Transmission Lines:I-Theory of Modal Analysis", IEEE Transactions on Power Apparatus and Systems, pp.200-205, March 1965.

13. George M. Swisher, Linear System Analysis, Matrix Publsihers Inc., Champaign, Ill., 1976.

APPENDIX

Table A-I.
34.5 KV Double Circuit Capacitor Component Values

Location	Actual Value[1]	Nominal Values[1]	Measured Values[1]			
			Chassis 1		Chassis 2	
			Side 1	Side 2	Side 1	Side 2
AB	288	270	274	274	274	274
		15	15.4	15.9	15.5	15.7
AC	151	150	152.5	152.2	152.2	152.4
AN	509	500	499	499	499	499
		10	10.5	10.5	10.5	10.5
BC	281	270	273	273	273	273
		10	10.5	10.5	10.5	10.5
BN	407	200	202	203	203	203
		200	202	202	202	202
CN	550	500	501	501	501	501
		47	46.2	46.6	46.1	46.1

[1]Values in pF

Table A-II.
34.5 KV Single Circuit Capacitor Component Values

Location	Actual Value[1]	Nominal Values[1]	Measured Values[1]			
			Chassis 1		Chassis 2	
			Side 1	Side 2	Side 1	Side 2
AB	64	47	46.7	45.7	46.2	46.0
		18	18.6	18.7	18.6	18.7
AC	83	82	82.6	82.8	83.3	82.5
AN	250	150	148.6	148.8	149.4	149.2
		100	100.4	100.5	100.5	100.5
BC	32	33	32.7	33.0	32.7	33.1
BN	219	200	199.0	198.7	199.1	199.1
		21	20.9	20.9	21.1	20.9
CN	242	200	202	202	202	202
		39	39.7	39.7	39.7	39.7

[1]Values in pF

Table A-III.
69 KV Double Circuit Capacitor Component Values

Location	Actual Value[1]	Nominal Values[1]	Measured Values[1]			
			Chassis 1		Chassis 2	
			Side 1	Side 2	Side 1	Side 2
AB	1929	1100	1095	1099	1100	1100
		820	829	829	828	828
AC	997	500	500	500	500	500
		500	497	498	497	497
AN	6518	4700	4560	4550	4550	4560
		2000	2010	2000	2030	2010
BC	2114	1500	1459	1449	1461	1459
		680	673	672	673	673
BN	4517	4700	4490	4490	4530	4500
CN	4759	4700	4770	4760	4780	4780

[1]Values in pF

Table A-IV.
69 KV Single Circuit Capacitor Component Values

Location	Actual Value[1]	Nominal Values[1]	Measured Values[1]			
			Chassis 1		Chassis 2	
			Side 1	Side 2	Side 1	Side 2
AB	2393	2200	2210	2220	2200	2210
		200	202	202	203	203
AC	1354	680	677	680	675	674
			679	674	679	681
AN	8174	6800	7000	6970	7010	6990
		1200	1197	1202	1196	1196
BC	2311	2200	2300	2300	2320	2300
BN	6084	4700	4570	4570	4580	4590
		1500	1527	1526	1523	1520
CN	7739	6800	7030	7050	7030	7020
		680	682	681	683	686

[1]Values in pF

Table A-V.
138 KV Double Circuit Capacitor Component Values

Location	Actual Value[1]	Nominal Values[1]	Measured Values[1]			
			Chassis 1		Chassis 2	
			Side 1	Side 2	Side 1	Side 2
AB	43.6	39	39.1	39.0	38.9	39.0
		2.2	2.25	2.25	2.25	2.25
		2.2	2.27	2.27	2.27	2.27
AC	22.56	150	22.6	22.5	22.5	22.5
AN	137.5	68	68.9	68.4	68.8	69.0
		68	68.4	68.8	68.5	68.3
BC	46.9	47	46.7	46.7	46.8	46.7
BN	96.7	68	67.9	67.9	67.9	67.9
		22	22.1	22.2	22.2	22.2
		68	6.83	6.85	6.82	6.82
CN	104.5	100	100.2	100.2	100.0	100.0
		4.7	4.68	4.80	4.69	4.67

[1]Values in 10^3 pF

Table A-VI.
138 KV Single Circuit Capacitor Component Values

Location	Actual Value[1]	Nominal Values[1]	Measured Values[1]			
			Chassis 1		Chassis 2	
			Side 1	Side 2	Side 1	Side 2
AB	44.7	39	39.1	39.2	39.3	39.3
		2.2	2.29	2.29	2.27	2.27
		2.2	2.35	2.33	2.33	2.33
		1.1	1.078	1.080	1.064	1.073
AC	39.4	39	39.4	39.4	39.3	39.4
AN	185.4	150	150.9	151.1	151.0	151.1
		33	33.7	33.5	33.5	33.5
BC	43.1	2.2	2.26	2.26	2.26	2.26
		39	39.2	39.2	39.2	39.2
		2.2	2.23	2.22	2.22	2.23
BN	168.4	100	99.8	99.8	99.7	99.7
		68	68.2	68.2	68.3	68.7
CN	185.3	150	149.7	149.1	148.9	150.2
		33	34.0	33.8	33.8	33.7

[1]Values in 10^3 pF

Table A-VII.
345 KV Double Circuit Capacitor Component Values

Location	Actual Value[1]	Nominal Values[1]	Measured Values[1]			
			Chassis 1		Chassis 2	
			Side 1	Side 2	Side 1	Side 2
AB	4.613	4.7	4.65	4.59	4.63	4.65
AC	2.281	2.2	2.28	2.28	2.28	2.28
AN	22.29	22	22.3	22.3	22.3	22.3
BC	5.423	4.7 .68	4.72 .684	4.79 .669	4.78 .670	4.74 .684
BN	15.10	15	15.20	15.21	15.29	15.27
CN	15.25	15	15.08	15.09	15.12	15.11

[1]Values in 10^{-3} uF

Table A-VIII.
345 KV Single Circuit Capacitor Component Values

Location	Actual Value[1]	Nominal Values[1]	Measured Values[1]			
			Chassis 1		Chassis 2	
			Side 1	Side 2	Side 1	Side 2
AB	8.30	6.8	6.81	6.81	6.81	6.82
		1.5	1.528	1.466	1.548	1.537
AC	3.163	1.2	1.213	1.213	1.210	1.210
		1.4	1.463	1.463	1.464	1.464
		.5	.498	.498	.501	.498
AN	56.82	33	33.3	33.3	33.3	33.3
		22	22.6	22.6	22.6	22.6
BC	7.34	6.8	7.41	7.10	6.95	6.97
				.267	.381	.381
BN	45.55	22	22.6	22.9	22.9	22.9
		22	22.9	22.6	22.6	22.6
CN	56.82	22	23.1	23.1	23.0	23.0
		33	32.8	32.8	32.9	32.9

[1]Values in 10^{-3} uF

Table A-IX.
765 KV Single Circuit Capacitor Component Values

Location	Actual Value[1]	Nominal Values[1]	Measured Values[1]			
			Chassis 1		Chassis 2	
			Side 1	Side 2	Side 1	Side 2
AB	191.1	68	67.8	67.8	67.7	67.7
		100	99.4	99.5	99.7	99.6
		22	22.7	22.7	22.7	22.7
AC	72.39	33	33.4	33.2	33.1	33.3
		39	39.2	39.2	39.2	39.2
AN	1445	470	470	471	473	473
		1000	996	980	975	977
BC	172	68	68.0	67.6	67.5	67.6
		33	33.1	33.0	32.7	32.6
		68	68.1	68.2	68.6	68.6
BN	1170	150	151.2	151.5	151.9	148.5
		1	1.002	1.006	1002	1001
CN	1445	470	463	464	476	466
		1000	1012	1011	1007	1008

[1]Values in 10^{-3} uF

Table A-X.
34.5 KV Circuit Coupling Capacitor Component Values

Location	Actual Value[1]	Nominal Values[1]	Measured Values Chassis 1 Side 1	Measured Values Chassis 1 Side 2
AA	166	150	153.4	153.6
		12	12.0	12.6
BB	101	100	100.2	100.2
CC	148	150	148.5	148.5
AB	131	120	121.7	121.7
		10	10.4	10.4
BC	124	120	122.3	122.3
CA	164	150	153.5	153.2
		10	10.7	10.8
AC	167	150	153.9	153.7
		12	12.0	12.1
BA	128	120	122.0	122.0
		5	5.6	5.7
CB	125	120	121.9	121.9
		5	5.0	5.0

[1]Values in pF

Table A-XI.
69 KV Circuit Coupling Capacitor Component Values

Location	Actual Value[1]	Nominal Values[1]	Measured Values[1] Chassis 1 Side 1	Measured Values[1] Chassis 1 Side 2
AA	937	820 100	831 100.9	831 101.6
BB	704	500 200	499 204	499 204
CC	1379	680 680	694 684	690 686
AB	871	820 39	831 39.5	831 39.9
BC	1034	1000 33	1004 33.5	1004 33.4
CA	1176	680 500	676 499	676 499
AC	1314	820 500	825 496	825 496
BA	779	500 270	509 268	504 274
CB	997	1000 10	984 10.2	984 10.4

[1] Values in pF

Table A-XII.
138 KV Circuit Coupling Capacitor Component Values

Location	Actual Value[1]	Nominal Values[1]	Measured Values[1] Chassis 1 Side 1	Measured Values[1] Chassis 1 Side 2
AA	18.76	15	14.76	14.75
		2	1.888	1.901
		2.2	2.24	2.13
BB	13.78	6.8	6.87	6.88
		6.8	6.90	6.90
CC	27.42	2.2	22.8	22.7
		4.7	4.66	4.66
AB	17.26	15	15.39	15.35
		2	1.963	2.04
BC	20.26	6.8	6.75	6.78
		6.8	6.77	6.77
		6.8	6.80	6.80
CA	23.43	22	23.2	23.3
AC	25.84	22	23.1	23.1
		2.2	2.29	2.33
BA	15.21	15	15.16	15.19
CB	19.81	2.2	2.23	2.24
		15	15.39	15.40
		2.2	2.24	2.23

[1]Values in 10^3 pF

Table A-XIII.
345 KV Circuit Coupling Capacitor Component Values

Location	Actual Value[1]	Nominal Values[1]	Measured Values[1] Chassis 1 Side 1	Measured Values[1] Chassis 1 Side 2
AA	1122	1100	1124	1126
BB	1286	1200 56	1231 57.1	1231 56.9
CC	3026	1500 1500	1466 1554	1466 1552
AB	1477	1500	1467	1467
BC	2187	1100 1100	1089 1094	1095 1088
CA	2308	2200 15	2290 16.0	2310
AC	2738	1500 1200	1520 1222	1218 1522
BA	1167	500 680	501 665	501 665
CB	2059	2000	2050	2050

[1]Values in pF

Table A-XIV.
34.5 KV Single Circuit Resistances

Phase	Chassis Type	Total Resistance	Inductor Resistance	Resistance to be Added	Resistance Used
A	1	3.34	0.40	2.94	3
B	1	3.67	0.48	3.19	4/20
C	1	3.67	0.40	3.27	4/20
N	1	2.62	0.32	2.3	5/4
A	2	3.34	0.40	2.94	3
B	2	3.67	0.48	3.19	4/20
C	2	3.67	0.40	3.27	4/20
N	2	2.62	0.32	2.3	4/5

Table A-XV.
34.5 KV Double Circuit Resistances

Phase	Chassis Type	Total Resistance	Inductor Resistance	Resistance to be Added	Resistance Used
A	1	3.27	0.40	2.87	3/47
B	1	3.46	0.48	2.98	3
C	1	3.75	0.40	3.35	4/20
N	1	5.01	0.46	4.55	5/47
A	2	3.27	0.40	2.87	47/3
B	2	3.46	0.48	2.98	3
C	2	3.75	0.40	3.35	4/20
N	2	5.01	0.46	4.55	5/47

Table A-XVI.
69 KV Single Circuit Resistances

Phase	Chassis Type	Total Resistance	Inductor Resistance	Resistance to be Added	Resistance Used
A	1	2.49	0.40	2.08	3/7.5
B	1	2.66	0.48	2.17	4/5
C	1	2.66	0.40	2.26	4/5
N	1	1.20	0.28	0.92	1/10
A	2	2.49	0.40	2.08	3/7.5
B	2	2.66	0.48	2.17	5/4
C	2	2.66	0.40	2.26	4/5
N	2	1.20	0.28	0.92	1/10

Table A-XVII.
69 KV Double Circuit Resistances

Phase	Chassis Type	Total Resistance	Inductor Resistance	Resistance to be Added	Resistance Used
A	1	1.47	0.40	1.07	1.5/4
B	1	1.52	0.48	1.04	2/3
C	1	1.64	0.40	1.24	2/3
N	1	2.09	0.19	1.9	2/40
A	2	1.47	0.40	1.07	1.5/4
B	2	1.52	0.48	1.04	1.5/4
C	2	1.64	0.40	1.24	2/3
N	2	2.09	0.19	1.9	2/40

Table A-XVIII.
138 KV Single Circuit Resistances

Phase	Chassis Type	Total Resistance	Inductor Resistance	Resistance to be Added	Resistance Used
A	1	2.39	0.32	2.07	3/7.5
B	1	2.53	0.32	2.21	4/5
C	1	2.39	0.32	2.07	3/7.5
N	1	1.15	0.28	0.87	1/7.5
A	2	2.39	0.32	2.07	3/7.5
B	2	2.53	0.32	2.21	4/5
C	2	2.39	0.32	2.07	3/7.5
N	2	1.15	0.28	0.87	1/7.5

Table A-XIX.
138 KV Double Circuit Resistances

Phase	Chassis Type	Total Resistance	Inductor Resistance	Resistance to be Added	Resistance Used
A	1	1.64	0.40	1.24	2/3
B	1	1.69	0.48	1.21	2/3
C	1	1.82	0.40	1.41	3/3
N	1	2.29	0.19	2.1	1.5/4+1
A	2	1.64	0.40	1.24	2/3
B	2	1.69	0.48	1.21	2/3
C	2	1.82	0.40	1.41	3/3
N	2	2.29	0.19	2.1	1.5/4+1

Table A-XX.
345 KV Single Circuit Resistances

Phase	Chassis Type	Total Resistance	Inductor Resistance	Resistance to be Added	Resistance Used
A	1	0.693	0.40	0.29	1/1/1
B	1	0.792	0.48	0.31	1/1/1
C	1	0.693	0.40	0.29	1/1/1
N	1	2.35	0.28	2.07	3/7.5
A	2	0.693	0.40	0.29	1/1/1
B	2	0.792	0.48	0.31	1/1/1
C	2	0.693	0.40	0.29	1/1/1
N	2	2.35	0.28	2.07	3/7.5

Table A-XXI.
345 KV Double Circuit Resistances

Phase	Chassis Type	Total Resistance	Inductor Resistance	Resistance to be Added	Resistance Used
A	1	0.590	0.40	0.19	.51/.51/.51
B	1	0.619	0.48	0.14	.51/.51/.51
C	1	0.709	0.40	0.31	1/1/1
N	1	1.59	0.36	1.23	2/3
A	2	0.590	0.40	0.19	.51/.51/.51
B	2	0.619	0.48	0.14	.51/.51/.51
C	2	0.709	0.40	0.31	1/1/1
N	2	1.59	0.36	1.23	2/3

Table A-XXII.
765 KV Single Circuit Resistances

Phase	Chassis Type	Total Resistance	Inductor Resistance	Resistance to be Added	Resistance Used
A	1	0.376	0.40	0	0
B	1	0.437	0.48	0	0
C	1	0.376	0.40	0	0
N	1	2.20	0.28	1.92	2/40
A	2	0.376	0.40	0	0
B	2	0.437	0.48	0	0
C	2	0.376	0.40	0	0
N	2	2.20	0.28	1.92	2/40

The vita has been removed from the scanned document